Scaling Effects on Damage Development, Strength, and Stress-Rupture Life of Laminated Composites in Tension

J. André Lavoie

Dissertation submitted to the Faculty of the Virginia Polytechnic Institute and State University
in partial fulfillment of the requirements for the degree of

Doctor of Philosophy
in
Engineering Mechanics

John Morton, Chair
William A. Curtin, Co-Chair
Kenneth L. Reifsnider
Karen E. Jackson
Don H. Morris
Mark S. Cramer

April 4th, 1997
Blacksburg, Virginia

Keywords: strength scaling, size effects, microcracking, first-ply failure, delamination, composite material, Weibull statistics, tension testing, flexural testing, carbon/epoxy, glass/epoxy, creep, stress-rupture, creep-rupture, stress relaxation, stress-corrosion cracking, durability, life.

Scaling Effects on Damage Development, Strength, and Stress-Rupture Life of Laminated Composites in Tension

J. André Lavoie

(ABSTRACT)

The damage development and strength of ply-level scaled carbon/epoxy composite laminates having stacking sequence of $[+\theta_n/-\theta_n/90_{2n}]_s$ where constraint ply angle, θ, was 0°, 15°, 30°, 45°, 60°, and 75°, and size was scaled as n=1,2,3, and 4, is reported in Part I. X-radiography was used to monitor damage developments. First-ply failure stress, and tensile strength were recorded. First-ply failure of the midplane 90° plies depended on the stiffness of constraint plies, and size. All 24 cases were predicted using Zhang's shear-lag model and data generated from $[0_2/90_2]_s$ cross-ply tests. Laminate strength was controlled by the initiation of a triangular-shaped local delamination of the surface angle plies. This delamination was predicted using O'Brien's strain energy release rate model for delamination of surface angle plies. For each ply angle, the smallest laminate was used to predict delamination (and strength) of the other sizes.

The in-situ tensile strength of the 0° plies within different cross-ply, and quasi-isotropic laminates of varying size and stacking sequence is reported in Part II. No size effect was observed in the strength of 0° plies for those lay-ups having failure confined to the gauge section. Laminates exhibiting a size-strength relationship, had grip region failures for the larger sizes. A statistically significant set of 3-point bend tests of unidirectional beams were used to provide parameters for a Weibull model, to re-examine relationship between ultimate strength of 0° plies and specimen volume. The maximum stress in the of 0° plies in bending, and the tensile strength of the of 0° plies (from valid tests only) was the same. Weibull theory predicted loss of strength which was not observed in the experiments.

An effort to model the durability and life of quasi-isotropic E-glass/913 epoxy composite laminates under steady load and in an acidic environment is reported in Part III. Stress-rupture tests of unidirectional coupons immersed in a weak hydrochloric acid solution was conducted to determine their stress-life response. Creep tests were conducted on unidirectional coupons parallel and transverse to the fibers, and on ±45° layups to characterize the lamina stress- and time-dependent compliances. These data were used in a composite stress-rupture life model, based on the critical element modeling philosophy of Reifsnider, to predict the life of two ply-level thickness-scaled quasi-isotropic laminates.

Keywords: strength scaling, size effects, microcracking, first-ply failure, delamination, composite material, Weibull statistics, tension testing, flexural testing, carbon/epoxy, glass/epoxy, creep, stress-rupture, creep-rupture, stress relaxation, stress-corrosion cracking, durability, life.

This work was supported by the US Army Research Laboratory under NASA grant NAS1-19610, No. 15, by the U.K. Ministry of Defence, and by the Virginia Institute for Material Systems.

ACKNOWLEDGMENTS

The author acknowledges the financial support of the US Army Research Laboratory for financial support under NASA grant NAS1-19610, No. 15, monitored by Dr. Karen Jackson. Additional financial support from the Virginia Institute for Material Systems, made possible by Prof. Ken Reifsnider, is gratefully acknowledged. Dr. Jackson's careful reading of drafts of my various papers was very helpful. A visit to the Royal Institute of Technology, Stockholm, was undertaken to collaborate with Professor Peter Gudmundson and his student, Erik Adolfsson, and would not have been possible without a tuition waiver. Erik was a pleasure to work with, and gave freely of his time. At the Structural Materials Centre (SMC), Defence Research Agency, in Farnborough, England, the author received support from many people in different groups while working on the stress-rupture project. Prof. Paul Curtis authorized composite plate fabrication, and Dr. Phil Powell arranged financing for Andrew Renshaw, a sandwich student, to help with creep and stress-rupture testing, and Mr. Bill Mitten allowed free access to the creep lab.

The author extends thanks to Dr. Costas Soutis at Imperial College for being a friend and taking special interest in the work. Dr. Paul Smith at the University of Surrey, Prof. Frank Jones at the University of Sheffield, Mr. Micheal G. Phillips at the University of Bath, and Dr. Paul Hogg at Queen Mary and Westfield College made time for helpful discussions. Prof. Kenneth L. Reifsnider provided helpful guidance during the literature review and proposal phase of the research, by steering me toward experimentation. The author is especially grateful to Dr. John Morton, committee chair and Director of the SMC, for providing me opportunities, especially the opportunity to spend one year pursuing my studies at the SMC. Prof. Bill Curtin, co-chair, provided further guidance, and help analyzing data.

The author wishes to thank his wife, Chiara, for her love and support during the long months of their separation while he pursued his research abroad. Her forgiveness is replied with a promise to avoid long separations again.

TABLE OF CONTENTS

Page

ABSTRACT....ii
ACKNOWLEDGEMENTS....iii
TABLE OF CONTENTS....iv
LIST OF TABLES....vii
LIST OF FIGURES....viii

Part I. Effects of Size, Constraint and Thickness, on Damage Initiation, Growth, and Strength of $[+\theta_n/-\theta_n/90_{2n}]_s$ Composite Laminates....1
Abstract....1
1. Introduction....2
2. Materials And Specimens....4
2.1. Materials And Laminates....4
2.2. Specimen Preparation....4
3. Analysis....6
3.1. Model for First-Ply Failure....6
3.2. Model for Stress-Strain Response while Laminate is Cracking....7
3.3. Model for Strength of Angle-Ply Laminates....8
4. Results....9
4.1. Thermal Stress-Induced Matrix Cracking....9
4.2. Mechanical Testing: Stress-Strain Response....11
4.3. First-Ply Failure: Effects of Constraint and Thickness....11
4.4. Effects of Constraint Ply Orientation on Interlaminar and Intralaminar Matrix Cracking Due to Tensile Loading....12
4.4.1. Damage Progression for Constraint Plies at ±15°....12
4.4.2. Damage Progression for Constraint Plies at ±30°....12
4.4.3. Damage Progression for Constraint Plies at ±45°....12
4.4.4. Damage Progression for Constraint Plies at ±60°....13
4.5. Damage and the Response of $[(+60/-60/90_2)_2]_s$ Lay-Up....13
4.6. Delamination of Surface $+\theta°$ Plies and Prediction of Strength....14
5. Discussion....15
5.1. First-Ply Failure....15
5.2. "Stitch" Crack Formation....16
5.3. Stress-Strain Response of the $[(+60/-60/90_2)_2]_s$ Lay-Up....17
5.4. Strength of $[+\theta_n/-\theta_n/90_{2n}]_s$ Laminates....17
6. Conclusions....17
7. References....18

Part II. Strength Scaling of Composite Laminates Amidst Invariant 0° Ply Strength 49
Abstract 49
1. Introduction 49
2. Materials and Specimens 52
3. Analysis 53
3.1. Prediction of 0° Laminae Strength Using Weibull Theory 53
3.2. Calculation of Stress in the 0° Plies 54
3.3. Calculation of Maximum Stress for the Three-Point Bend Test 55
4. Results 56
4.1. Three-Point Bend Tests 56
4.2. Tensile Test Results with Comparison to Weibull Prediction 57
4.2.1. Tensile Tests of $[0]_{8n}$ and $[0_{2n}/90_{2n}]_s$ 57
4.2.2. Tensile Tests of $[90_n/0_n/90_n/0_n]_s$, $[90/0/90/0]_{ns}$, and $[+45/-45/0/90]_{ns}$ 58
4.2.3. Tensile Tests of $[+45_n/-45_n/0_n/90_n]_s$ 59
4.3. Width and End Tab Effects on Strength of $[+45_n/-45_n/0_n/90_n]_s$ 60
4.3.1. Effect of Specimen Width on Strength 60
4.3.2. Effect of End Tab on Strength 61
5. Discussion 62
5.1. Grip Failures in the $[0]_{8n}$ and $[0_{2n}/90_{2n}]_s$ Specimens 62
5.2. Stress Concentration Due to 90° Matrix Cracks 62
5.3. Adjustments Made to Strain Data 63
5.4. Stiffness Change, Failure Strain and Laminate Strength 63
5.5. Error in Extending Weibull Theory to Unidirectional Composites 63
5.6. Explanation for Grip Failures in Unidirectional Composites 64
5.7. Future Work: Improved Unidirectional Strength Test Methods 64
6. Conclusions 65
7. References 66

Part III. Prediction of Stress-Rupture Life of Glass/Epoxy Laminates in an Acidic Environment from Lamina Behavior 87
Abstract 87
1. Introduction 87
2. Experiments 88
2.1. Materials and Specimen Preparation 88
2.2. Quasi-Static Tensile Testing 90
2.3. Creep and Stress-Rupture Testing 90
2.3.1. Strain Measurement 90
2.3.2. Environmental Conditioning 90
2.3.3. Creep Tests 91

2.3.4. Stress-Rupture Tests....91
3. Stress-Rupture Life Modeling....91
3.1. Estimation of Remaining Strength and Life....92
3.2. Modeling Loss of Strength in the Unidirectional Plies....93
3.3. Creep Model of Compliance Change....94
3.4. Other Mechanisms Influencing Life....95
4. Results....95
4.1. Quasi-Static Strength Tests and Damage Characterization....95
4.1.1. Unidirectional $[0]_8$ Specimens....95
4.1.2. Quasi-Isotropic Specimens....95
4.2. Viscoelastic Creep Tests....96
4.2.1. Lamina Creep Characterization....96
4.2.2. Quasi-Isotropic Creep Data and Predictions....97
4.3. Stress-Rupture Tests and Damage Developments....98
4.3.1. Stress-Rupture of Unidirectional $[0]_2$ Specimens....98
4.3.2. Stress-Rupture of Quasi-Isotropic $[0/90/+45/-45]_s$ Specimens....99
4.4. Stress-Rupture Life Predictions....100
5. Discussion....100
5.1. Quasi-Static Tensile Strength Data....100
5.1.1. Unidirectional $[0]_8$ Tensile Tests....100
5.1.2. Quasi-Isotropic Specimens....101
5.2. Creep Test Data....101
5.2.1. Unidirectional $[0]_2$ Creep Tests....102
5.2.2. Fitting Curves to the $[+45/-45/+45/-45]_s$ Creep Tests....102
5.2.3. Moisture Absorption Effects on Creep Response and Life....102
5.3. Stress-Rupture Life....103
5.3.1. Experimental Variability....103
5.3.2. Model Predictions....103
5.3.3. Effect of "n" on Stress-Rupture Life of $[0]_n$ Unidirectional Specimens....103
5.3.4. Other Damages to the Sub-Critical Elements: Observed, Yet Unaccounted For....104
5.4. Future Work....104
6. Conclusions....105
7. References....105
Appendix: Stress-Rupture Life FORTRAN Code....140
Vita....145

LIST OF TABLES

Part I

Table 1. Specimen sizes and dimensions 23
Table 2. Mechanical properties of $[+\theta_n/-\theta_n/90_{2n}]_s$ laminates for differing size, n 23
Table 3. Thermal stress-induced 90° crack density of $[+\theta_n/-\theta_n/90_{2n}]_s$ 23
Table 4. Count of thermal stress-induced cracks in $+\theta°$ plies 23
Table 5. Length and density of cracks in $-\theta°$ plies 24
Table 6. Stiffnesses and strain energy release rate for delamination of $+\theta°$ plies 24
Table 7. Experimental results for strength of $[+\theta_n/-\theta_n/90_{2n}]_s$ laminates 25

Part II

Table 1. Specimen dimensions 68
Table 2. Detail about end tabs used on quasi-isotropic $[+45_n/-45_n/0_n/90_n]_s$ specimens 68
Table 3. Unidirectional $[0]_{8n}$ strength, and failure strain 68
Table 4. Unidirectional $[0]_{8n}$, strength, failure strain, and location of failure 69
Table 5. Cross-ply $[0_{2n}/90_{2n}]_s$ strength, failure strain, and 0° stress 69
Table 6. Cross-Ply $[0_{2n}/90_{2n}]_s$, strength, failure strain, and location of failure 70
Table 7. Cross-ply $[90_n/0_n/90_n/0_n]_s$ strength, failure strain, and 0° stress 70
Table 8. Cross-ply $[90/0/90/0]_{ns}$ strength, failure strain, and 0° stress 71
Table 9. Quasi-isotropic $[+45/-45/0/90]_{ns}$ strength, failure strain, and 0° stress 71
Table 10. Quasi-isotropic $[+45_n/-45_n/0_n/90_n]_s$ strength, failure strain, and 0° stress (Johnson) 72
Table 11. Quasi-isotropic $[+45_n/-45_n/0_n/90_n]_s$ strength, failure strain, and 0° stress (Kellas) 72
Table 12. Quasi-isotropic $[+45_n/-45_n/0_n/90_n]_s$ strength, failure strain, and location of failure 73
Table 13. Experimental results for ultimate strength of scaled $[+45_n/-45_n/0_n/90_n]_s$ laminates 74
Table 14. Effect of end tab on strength of quasi-isotropic $[+45_n/-45_n/0_n/90_n]_s$ specimens 74

Part III

Table 1. Elastic and strength properties of E-glass/913 108
Table 2. Elastic properties of E-glass/913 from creep test data 108
Table 3. Stress-rupture life results 109

LIST OF FIGURES

Part I.

Figure 1. X-ray of fabrication microcracks in the $[+15_4/-15_4/90_8]_s$ layup 26
Figure 2. X-ray of fabrication microcracks in the $[+30_4/-30_4/90_8]_s$ layup 27
Figure 3. X-ray of fabrication microcracks in the $[+45_4/-45_4/90_8]_s$ layup 28
Figure 4. Typical stress/strain plots for $[+\theta_n/-\theta_n/90_{2n}]_s$ laminates....29
Figure 5. Plots of first-ply failure of $[+\theta_n/-\theta_n/90_{2n}]_s$ laminates....30
Figure 6. Development of -15/90 interface failure at 90° crack tips....31
Figure 7. Edge view of inclined secondary cracks in the 90° plies, with 90° crack-tip delaminations and continuous -15/90 interface delamination....32
Figure 8. X-ray of localized delaminations associated with the -15/90 local delamination....33
Figure 9. Edge view of development of -30/90 delamination from the 90° crack 34
Figure 10. X-ray of deep delamination of the -30/90 interface along 90° crack tips 35
Figure 11. X-ray of effect of edge polish on damage sequence in a $[+30/-30/90_2]_s$ layup....36
Figure 12. Edge view of growth of a -30° crack from a 90° crack at the -30/90 interface....37
Figure 13. Internal section showing cracks in a $[+45_4/-45_4/90_8]_s$ laminate, before loading....38
Figure 14. Internal section of a $[+45/-45/90_2]_s$ specimen loaded to failure....39
Figure 15. An internal section of a $[+45_2/-45_2/90_4]_s$ laminate 40
Figure 16. X-ray of 90° cracks and -60° stitch cracks in a $[+60/-60/90_2]_s$ layup....41
Figure 17. X-ray, 90° cracks and +/-60° cracks in a $[+60/-60/90_2]_s$ layup, loaded further....41
Figure 18. Edge view of a $[(+60/-60/90_2)_2]_s$ laminate 42
Figure 19. X-ray of cracks in a sublaminate-scaled $[(+60/-60/90_2)_2]_s$ laminate....43
Figure 20. Modeled vs. actual stress/strain response of $[(+60/-60/90_2)_2]_s$ laminate....44
Figure 21. X-ray of +15° delaminations....45
Figure 22. X-ray of +45° delaminations....46
Figure 23. Photographs of failed $[+\theta_3/-\theta_3/90_6]_s$ laminates....47
Figure 24. The strength scaling of $[+\theta_n/-\theta_n/90_{2n}]_s$ laminates 48

Part II.

Figure 1. Schematic of the 3-point bend test....75
Figure 2. Fracture profile of a 3-point bend specimen 75
Figure 3. Typical load vs. displacement trace for a 3-point bend test....76
Figure 4. Survivability vs. stress for unidirectional $[0]_{32}$ beams in 3-point bending 77
Figure 5. Stress vs. strain plots of $[0_{2n}/90_{2n}]_s$ 78
Figure 6. Plot of stress at failure of 0° plies for unidirectional $[0]_{8n}$ and $[0_{2n}/90_{2n}]_s$ 79

Figure 7. Plot of stress at failure of 0° plies for $[90_n/0_n/90_n/0_n]_s$, $[90/0/90/0]_{ns}$, and quasi-isotropic $[+45/-45/0/90]_{ns}$ 80
Figure 8. X-ray of delamination in $[+45_n/-45_n0_n/90_n]_s$ layups loaded near failure 81
Figure 9. Constraint effect on the fracture profile for two sizes of quasi-isotropic layups 82
Figure 10. Typical grip failures for the $[+45_3/-45_3/0_3/90_3]_s$ laminate 83
Figure 11. Plot of stress at failure of 0° plies for $[+45_n/-45_n/0_n/90_n]_s$ coupons.....84
Figure 12. Strength of the $[+45_n/-45_n/0_n/90_n]_s$ laminate for different thickness and width 85
Figure 13. Representative stress vs. strain plots of $[+45_n/-45_n/0_n/90_n]_s$ 86

Part III.

Figure 1. Creep frame with specimen and extensometers.....110
Figure 2(a). 0° specimen showing clamped end tabs.....111
Figure 2(b). Alignment fixture for end tabs.....112
Figure 3. Close-up view of the acid cell.....113
Figure 4(a). Fracture of $[0]_8$ quasi-static tensile specimen.....114
Figure 4(b). Representative fracture profile of a quasi-static tensile test of $[0/90/+45/-45]_s$ E-Glass/913-epoxy laminate.....115
Figure 4(c). Representative fracture profile of a quasi-static tensile test of $[0_2/90_2/+45_2/-45_2]_s$ E-Glass/913-epoxy laminate.....116
Figure 5. Creep results for constant stress tests of $[0]_2$ E-glass/913-epoxy in 0.01 molar HCl acid bath.....117
Figure 6. Creep results for 200 MPa constant stress tests of $[0]_2$.....118
Figure 7. Creep results for constant stress tests of $[0]_2$ 119
Figure 8. Linearized Findley fit to $S_{11}(t)$ compliance vs. time data.....120
Figure 9. Examination of quality of fit early in the life for S_{11} 121
Figure 10. Linearized Findley fit to experimentally determined $S_{22}(t)$ vs. time data.....122
Figure 11. Schapery's quadratic fitting function fit to $S_{66}(t)$ data 123
Figure 12. Creep results for 128 MPa constant stress tests of $[0/90/+45/-45]_s$ 124
Figure 13. Creep results for 112 MPa constant stress tests of $[0/90/+45/-45]_s$ 125
Figure 14. Creep results for 80 MPa constant stress tests of $[0/90/+45/-45]_s$ 126
Figure 15. Creep results for 154 MPa constant stress tests of $[0_2/90_2/+45_2/-45_2]_s$ 127
Figure 16. Creep results for 124 MPa constant stress tests of $[0_2/90_2/+45_2/-45_2]_s$ 128
Figure 17. Creep results for 108 MPa constant stress tests of $[0_2/90_2/+45_2/-45_2]_s$ 129
Figure 18. Predicted and experimental creep vs. time response of quasi-isotropic layup.....130
Figure 19. Representative fracture profile of stress-ruptured $[0]_2$ having a higher stress (225 MPa), and shorter life (18.7 hours).....131
Figure 20. Representative fracture profile of stress-ruptured $[0]_2$ layup having a lower stress (185 MPa), and longer life (41 hours).....132

Figure 21. Fit to experimentally determined $[0]_2$ stress-rupture life data.....133
Figure 22. Representative fracture profile of stress-ruptured $[0_2/90_2/+45_2/-45_2]_s$ having a higher stress (154 MPa), and shorter life (13.0 hours).....134
Figure 23. Schematic of the formation of a stress-corrosion crack in the surface 0°-ply.....135
Figure 24. Representative fracture profile of stress-ruptured $[0/90/+45/-45]_s$ layup 136
Figure 25. Representative fracture profile of stress-ruptured $[0_2/90_2/+45_2/-45_2]_s$ layup 137
Figure 26. Prediction of the life of a $[0/90/+45/-45]_s$ laminate 138
Figure 27. Prediction of the life of a $[0_2/90_2/+45_2/-45_2]_s$ laminate 139

Part I

Effects of Size, Constraint and Thickness, on Damage Initiation, Growth, and Strength of $[+\theta_n/-\theta_n/90_{2n}]_s$ Composite Laminates

Abstract

An experimental investigation of damage development and strength was conducted on ply-level scaled carbon/epoxy composite laminates having stacking sequence of $[+\theta_n/-\theta_n/90_{2n}]_s$ where the constraint ply angle, θ, was 0°, 15°, 30°, 45°, 60°, and 75°, and size was scaled as n=1,2,3, and 4. Photomicrography and x-radiography were used to monitor damage development with tensile load. Subcritical damage development before complete failure was dependent upon the constraint ply angle, θ, for their mode, but the size affected the initiation stress, and rate of development. Damage in the form of high density matrix cracking in plies adjacent to plies with a major matrix crack appeared due to thermal residual stress, and after monotonic loading. To highlight the significance of the failure mode on elastic properties of particular damaged lay-ups, the $[(+60/-60/90_2)_2]_s$ lay-up was tested, and its stress-strain response compared to that predicted from Gudmundson's model (Gudmundson, Östlund, and Zang, 1993).

Measurements of first-ply failure stress, and tensile strength were made. First-ply failure of the midplane 90° plies was shown to depend on the level of constraint, and the scale factor, n. The strain energy release rate for matrix microcracking was computed from first-ply failure data of the $[0_2/90_2]_s$ laminate. Then, first-ply failure was predicted from Zhang's model (Zhang, Fan, and Soutis, 1993) for all other lay-ups and sizes, accounting for both constraint and size. Tensile strength was predicted using O'Brien's strain energy release rate model for delamination of surface angle plies. A delamination energy value for each ply angle was calculated from the smallest (n=1) laminates to predict delamination (and strength) of the n=2, 3, and 4 sizes. The predictions were successful because strength was controlled by the initiation of a triangular-shaped local delamination of the surface angle plies.

Keywords: strength scaling, size effect, matrix microcracking, first-ply failure, delamination, carbon/epoxy composite material, laminated composite material.

1. Introduction

The problem of matrix cracking in composite materials is usually not that it is a cause for some impending structural failure, but that these cracks can act as stress raisers, and are initiation sites for more critical damage such as delamination. Cracks can allow ingress of the environment, which is often deleterious. The motivations for the work contained in this report originates with observations that matrix microcracking in the transverse, or 90°, plies of cross-ply composite laminates in tension did not initiate at the same stress as that measured in a transverse tension test. Instead, the stress to crack the 90° plies varies as a function of the constraint imposed by the sandwiching plies, and the thickness of both constraint and constrained plies.

A 2-D elasticity analysis of a three ply laminate for the case of a single crack in the middle ply was given by Vasil'ev (1970). Each ply could be orthotropic, and a saturation crack spacing could be predicted. An equilibrium element approach (1-D shear-lag model) was used by Reifsnider (1977) and Highsmith and Reifsnider (1982), to analyze the role of the constraining plies on the development of cracks in the interior constrained plies, to predict the saturation crack spacing, and to give information on stress concentration in the constraint plies. Parvizi, Garrett, and Bailey (1978) tested cross-ply laminates of the form $[0/90_n]_s$ where n=1,2,3,... They modeled the crack initiation using a 1-D shear lag model and a Griffith energy balance concept extended from the theory of Aveston and Kelly. Flaggs and Kural (1982) tested $[0_2/90_n]_s$, $[\pm 30/90_n]_s$, and $[\pm 60/90_n]_s$, where n=1,2,4, and 8, to investigate the effect of constraint on cracking. They showed that the models of the time had difficulty predicting the onset of cracking except in the most constrained cases. They also showed that the material system could not be characterized as a simple Weibull material. Fukunaga *et al.* (1984) used a statistical strength analysis together with a shear-lag analysis to predict first ply failure of the $[\pm\theta/90_n]_s$ laminates described by Flaggs and Kural. Kistner, Whitney, and Browning (1985) confirmed that the "in situ" strength variation of the transverse plies was real in the sense that the orientation of the constraining plies affected the strain at which cracking initiates. They tested unidirectional laminates ranging in thickness from four to sixteen plies in transverse tension, and showed that the thickness, in and of itself, had no effect on transverse strength. However, O'Brien and Salpekar (1993) found that the transverse tensile strength did obey a Weibull volumetric scaling law. Crossman and Wang (1982) studied damage initiation and growth in $[\pm 25/90_n]_s$ laminates where n=1,...,8. The first damage to initiate depended upon n. A finite element energy analysis could predict onset of transverse cracking. Dvorak and Laws (1987) attempted to predict the growth of a transverse crack within the ply, parallel to the fibers, and toward the ply interfaces. Zhang, Fan, and Soutis (1992) presented a model based on classical fracture mechanics and assuming a through-thickness flaw. The model used a modified 2-D shear-lag analysis wherein shear stresses were allowed to vary linearly within the constraining plies and cracked 90° plies. Hashin (1985) used variational methods to account for crack interaction and predicted changes in axial Young's modulus, and Poisson's ratio. Varna and Berglund (1991, 1993) found unacceptably large errors in Hashin's analysis for Poisson's

ratio prediction, due to the approximate stress field chosen, improved upon his work, and resolved the problem of accurate stress field determination. Gudmundson and coworkers (1992, 1993) have developed a general model for estimating the thermoelastic properties of arbitrary composite laminates having cracks in any ply, and any crack density. The model depends upon a closed form solution for the crack opening displacements in an infinite isotropic medium. Most elastic properties, thermal expansion coefficients, and elastic coupling coefficients are computed. The model does not predict crack initiation, but must be given the strain energy release rate for cracking and resistance curve for progressive cracking. Talreja (1985a,b) developed a continuum damage mechanics modeling approach, where the mechanical response of a damaged composite material is characterized by a set of vector fields each representing a damage mode. Recently, Talreja (1996) proposed a combined approach to structural analysis in which the strengths of micromechanics to compute accurate local displacements in damaged materials is combined with continuum damage mechanics useful to compute laminate level thermoelastic property changes.

Several types of delamination were encountered during the course of this work, and have all been studied previously. These are gross edge delamination, crack-tip induced interply delamination, and triangular-shaped local delaminations in off-axis plies. The large edge delamination characterized by interply separation along the length of the gauge section of a composite coupon specimen, for example, often involves a substantial portion of the width. This kind of delamination has received much attention, and some works are by O'Brien (1982a,b), Kim and Soni (1984), and Lagace (1987). Not to be neglected are works which look at the conditions which favor the development of edge delamination. Edge stresses and edge effects were studied by Pipes and Pagano (1970, 1973), Pipes and Daniel (1971), Pagano and Pipes (1973), Oplinger, Parker, and Chiang (1974), Hsu and Herakovich (1977), Rodini and Eisenmann (1978), Curtis (1980), Herakovich, Post, Buczek, and Czarnek, (1985), and Herakovich (1981,1982).

The development of delamination at the interface of the cracked and the constraining plies is described by Reifsnider, Henneke, Stinchcomb, and Duke (1983), Jamison, Schulte, Reifsnider, and Stinchcomb (1984), and Crossman and Wang (1982), among others. Talreja (1986) employed continuum damage mechanics to model the property changes that result. Zhang, Soutis, and Fan (1994a,b) use a combined fracture mechanics and finite element model to compute the total strain energy associated with this form of delamination at the edge. Wang and Karihaloo (1994) solved for the stress intensity factor to cause delamination due to a matrix crack. The triangular delamination was observed by Herakovich (1982), and O'Brien and Hooper (1993). A model to predict the onset of the triangular delamination was developed by O'Brien (1993).

In the current work, damage development, and ultimate strength of composite laminates was studied from the scaling viewpoint. Specifically, the dimensions were varied in length, width, and most importantly, thickness. Thickness was usually scaled in two ways: ply-level scaling in

which plies of the same orientation are clustered together, and sublaminate-level scaling in which a stacking sequence is repeated any number of times to build up the laminate thickness. Some works which consider thickness scaling are by Rodini and Eisenmann (1978), Crossman and Wang (1982), Herakovich (1982), Kellas and Morton (1990,1992), Kellas, Johnson, Morton, and Jackson (1993), and Jackson and Kellas (1993).

The work of Jackson and Kellas (1993) was an experimental investigation of damage development and strength of ply-level scaled carbon/epoxy composite laminates having stacking sequence of $[+\theta_n/-\theta_n/90_{2n}]_s$ where constraint ply angle, θ, was 0°, 15°, 30°, 45°, 60°, and 75°, and size was scaled as n=1,2,3, and 4. In addition, they tested the sublaminated-level scaled $[(+\theta/-\theta/90_2)_2]_s$ layup, where θ varied as before. The results reported were on initial modulus and ultimate strength. The purpose of their work was to investigate the effect of outer ply constraint (the $[+\theta_n/-\theta_n$ ply group) on the initial modulus and tensile strength of the coupons. Strength was shown to vary markedly as a function of thickness, n. The current paper is a continuation of the work begun by Jackson and Kellas (1993). The focus here, was to characterize the nature and sequence of the damages developed, such as those described previously, to isolate the mechanism(s) governing strength and to attempt to model the onset of various damage modes and strength, especially accounting for the effect of size. Furthermore, the $[(+60/-60/90_2)_2]_s$ layup was singled out for added attention because of its remarkable plastic-like stress-strain response.

2. Materials and Specimens

2.1. MATERIALS AND LAMINATES

The material used for this study was a commonly available 0.125 mm thick unidirectional graphite/epoxy prepreg: Hercules Magnamite AS-4/3502. Laminates were cured at 177°C. A range of laminates were fabricated. They were ply-level scaled laminates having the stacking sequence $[+\theta_n/-\theta_n/90_{2n}]_s$, where θ varied from 0° to 75° in 15° steps. Laminate thickness, width, and length was changed by varying "n" from 1 to 4. There was also a 16-ply laminate having stacking sequence of $[(+60/-60/90_2)_2]_s$. Specimen dimensions appear in Table 1.

2.2. SPECIMEN PREPARATION

Specimens were machined from flat panels using a high speed diamond saw with liquid cooling. This machining operation resulted in very smooth, square cuts. One edge of each specimen was polished so that cracks and delaminations could be readily discerned. A special polishing procedure was needed to polish the entire specimen's edge. First, to help keep the specimen edge flat against the grinding surface, three to five specimens were clamped together. It was possible to begin the wet grinding with #400 grit silicon carbide paper because the edges were

cut very square and flat during the machining operation. Flatness had to be maintained at each step in the grinding process for the final polish to result in a high quality finish. To ensure flatness, the block of specimens was ground by hand against a large flat surface using a fore and aft motion with the specimens aligned to the grinding direction. Grit and debris were flushed out with running water, followed by immersion in an ultrasonic bath. The second step was carried out using an Engis Corporation Hyprez lapping system. A copper lapping platen, 38 centimeters in diameter, and turning at 50 revolutions per minute (rpm), was sprayed with a 3 μm diamond slurry (formula 3(S4305-6) STD-MA). The diamond was carried in a low viscosity petroleum distillate, having a texture of light oil, but with the property of evaporating away within minutes. Polishing took about 3 minutes when the platen's surface was freshly prepared. Final polish was on a polishing wheel covered with a hard and flat cloth, such as Kempad "Pan-W" PSA. The polishing compound was a 0.3 μm alumina suspension, such as Struers code SDALOC-.3. Polishing took about a minute, when a wheel speed of about 150 rpm was used.

Mechanical Testing These laminates did not suffer from grip region stress concentration which might adversely affect strength, and so end tabs were not needed. Specimen ends were covered with a #100 grit cloth, which was sufficient to protect the fibers from damage by the grip face, yet still provide the needed traction. All data reported are for specimens from the same batch of material. Each panel yielded twelve specimens. Six specimens per panel were used to determine strength and initial elastic modulus, by Jackson and Kellas (1993). Their data was used here, and appears in Table 2. The remaining specimens were used to study damage development. To verify that there was not a significant difference in the test methods used, one specimen each from the remaining six specimens, was tested to failure. For those tests the test conditions were as follows. The test machine was a screw driven Instron. Specimens were gripped in Instron hand-tightened wedge-action grips. The crosshead speeds were chosen according to the specimen size to give a constant strain rate of 0.5% strain per minute, which translated to 2.54 x n mm/minute (where n = 1, 2, 3, or 4). The elastic modulus data presented was determined by Jackson and Kellas (1993) using back-to-back strain gages located at the geometric center of the specimen.

First-ply failure was determined by listening for the onset of matrix microcracking in the 90° plies, striking the "unload" button on the test machine, and recording the peak load from the test machine's memory. For this study, first-ply failure was the stress to initiate a 90° matrix crack, regardless of whether there were pre-existing cracks. To characterize damage developments beyond first ply failure, specimens were loaded to intermediate stress levels below failure, and x-rays were taken to observe the damage developed. Damage was monitored by occasionally removing the specimen and inspecting the polished edge for cracks and delamination. Dye penetrant enhanced x-radiography was used to peer inside the laminate to determine the extent of delamination and the nature of the matrix cracking. The recipe for the x-ray dye penetrant was to dissolve 60 grams of zinc iodide in 10 ml each of water, ethanol, and Kodak Photo-Flo 200.

Two methods were used for taking x-rays after loading specimens to the desired stress level. The first method involved removing the specimen from the tensile test machine, submerging it in the dye penetrant for at least 1/2 hour, then carefully cleaning the entire specimen. Failure to completely clean the specimen resulted in clouded or foggy x-rays. Specimens were then arranged on a sheet of Kodak Industrex SR5, or Industrex M5 x-ray film inside an Hewlett Packard Faxitron series 43805N x-ray cabinet. The film was processed using Kodak GBX developer and fixer. Besides being time consuming and messy, this method had the drawback that when the specimen was unloaded the cracks would close. Even with a long soak time, dye penetration may have been incomplete. The second method of obtaining x-radiographs had the advantage of speed, cleanliness, and assured penetration of the dye. The specimen was loaded to the desired stress level, then unloaded slightly (about 20%) to ensure that failure would not occur while preparing the specimen for x-ray, or during the x-ray exposure. Dye penetrant was introduced to both edges of the specimen using a syringe and a bead of penetrant was allowed to drip along the specimen length. Immediately after, a sheet of Polaroid Type 52 (ISO 400), or Type 55 (ISO 50), black and white film was taped to the specimen and exposed using a portable x-ray system. The convenience of the Polaroid film was undermined by its low resolution for this task. Resolution was adequate to reveal all damage except for very fine cracks having the appearance of stitches. X-rays were repeated, as needed, using the Kodak Industrex film described earlier, to highlight the missing details.

3. Analysis

The topics of matrix cracking and delamination, both investigated in this study, were two areas that have had a great deal of attention from the modeling community, therefore it would have been unwise to spend additional time on model development. Even reproducing the models from the literature, in order to test them against the experimental results, was highly time consuming. Of the three models eventually used, only O'Brien's (1993) had a simple closed-form solution that was easily implemented. The other two models were complex computer models that would have been prohibitively time consuming to reconstruct. Therefore, gaining direct access to the models was well worth the effort involved. The author was fortunate to have been given the computer code for the model of Zhang, Fan and Soutis (1992) and was provided with the resources for an on-site visit to use the model of Gudmundson, Östlund, and Zang (1992).

3.1. MODEL FOR FIRST-PLY FAILURE

The equivalent constraint model (ECM) is a 2-D shear-lag model used to predict in-plane stiffness properties for laminates of the general type $[\pm\theta_m/90_n]_s$ which contain 90° matrix cracks, Zhang, Fan and Soutis (1992). In the current study, the ECM was used to predict first-ply failure as a function of constraint ply angle and laminate size. The ECM allowed for out-of-plane shear

deformation in the constraining plies. In contrast, the 1-D shear-lag models assumed constant in-plane displacements across the thickness of the constraint plies, and confined shear stress transfer to a resin-rich interply layer. This distinction between the 1-D and 2-D models becomes increasingly significant when the constraint plies are oriented off-axis. As the constraint ply angle, θ, increases, the out-of-plane shear modulus, G_{23} (on the order of 50 to 60% that of G_{12}) becomes the dominant shear modulus, in preference to G_{12}. Hence, as the shear moduli of constraint layers and constrained layers converges, the assumption of constant in-plane displacements becomes increasingly inaccurate. Another refinement to the model was to allow partial linear variation of the shear stresses across the constraining plies. This approach was more realistic than using the entire constraint ply group thickness because stress perturbations are generally thought to dissipate within a typical ply thickness. Here, the model was set to confine the shear stress in the constraining plies to vary linearly over a single ply thickness for all sizes of laminates.

In order to predict the initiation of first-ply failure, the model needed the material elastic properties, residual thermal stresses, and the strain energy release rate, G, for transverse matrix cracking. Obtaining elastic properties was not difficult. However, the residual stress state was unknown because there was substantial stress relaxation, especially immediately after fabrication. Use of the difference between the cure and room temperature would give an overly high estimate of residual stress. For that reason, model predictions assuming no stress relaxation, and complete stress relaxation, were included.

The $[0_2/90_2]_s$ cross-ply lay-up (n=1) was chosen to determine the strain energy release rate, G. Then, the model was used to predict first-ply failure stress as a function of constraint ply angle, θ, and laminate size, n.

3.2. MODEL FOR STRESS-STRAIN RESPONSE WHILE LAMINATE IS CRACKING

Gudmundson and coworkers have produced a model capable of predicting the onset and growth of matrix cracking in each and every ply of an arbitrary composite laminate, and the thermoelastic property changes as a consequence. The general nature of the model made it the best available choice for the task of modeling the stress-strain response of laminates which exhibit matrix cracking in arbitrary layers. The response of the $[(+60/-60/90_2)_2]_s$ lay-up was highly nonlinear due to the development of dense matrix cracking. The purpose of modeling the stress-strain response of this laminate was twofold. First, this lay-up would provide a harsh test of the model, and second, to highlight the effect of a particularly dense form of microcracking on laminate stiffness.

The model was given an initial strain energy release rate for matrix microcracking, G, of 100 J/m^2. Past research which investigates crack multiplication, has shown that there is an

increasing resistance to continued cracking as the matrix crack density increases. A resistance curve was used for G(r) and was assumed to be:

$$G(r) = 100\left(1 + \sqrt{r}\right). \tag{1}$$

The variable, r, is crack density normalized by the thickness of the cracked layer. The form chosen for G(r) was based upon that of similar carbon/epoxy materials. Attention was given to forcing the onset of matrix cracking in the midplane 90° plies of the model to coincide with that of the experimental data. The value for G was assumed to be the same for all plies in the laminate, regardless of their orientation or thickness.

3.3. MODEL FOR STRENGTH OF ANGLE-PLY LAMINATES

Catastrophic failure of $[+\theta_n/-\theta_n/90_{2n}]_s$ laminates was identified to occur upon initiation of a triangular-shaped delamination of the surface +θ° angle plies from a +θ° matrix crack at the free edge. The analysis of O'Brien (1993) gives an expression for the strain energy release rate, G, for such local delaminations growing from an arbitrary angle ply matrix crack as:

$$G = \frac{P^2}{2mw^2}\left(\frac{1}{t_{LD}E_{LD}} - \frac{1}{tE_{LAM}}\right) \tag{2}$$

Here, m=1 because delamination initiates from one +θ° crack on one side of the laminate, not on both sides simultaneously. The expression in Equation 2 can be rewritten as:

$$G = \frac{N_x^2}{2h}\left(\frac{1}{(N-n)E_{LD}} - \frac{1}{NE_{LAM}}\right) \tag{3}$$

symbols, definitions, and units:
G = strain energy release rate for local delamination, J/m^2
N_x = tensile force resultant on the laminate, N/m
h = ply thickness, m
N = number of plies in the laminate
n = number of plies in the locally delaminated region
E_{LAM} = modulus of the laminate, Pa
E_{LD} = modulus of the locally delaminated region, Pa

The general expression for E_{LD} given by O'Brien handles unsymmetric delaminated sublaminates and is:

$$E_{LD} = \frac{2}{(N-n)h}\left[A_{11} - \left(\frac{A_{12}D_{22} - B_{12}B_{22}}{A_{22}D_{22} - B_{22}^2}\right)A_{12} + \left(\frac{A_{12}B_{22} - A_{22}B_{12}}{A_{22}D_{22} - B_{22}^2}\right)B_{12}\right] \quad (4)$$

The laminates in this study all had symmetric delaminated sublaminates, and as a consequence there is no bend extension coupling, therefore the B_{ij} terms are all zero and the expression for E_{LD} in Equation 4 simplifies to:

$$E_{LD} = \frac{2}{(N-n)h}\left(A_{11} - \frac{A_{12}^2}{A_{22}}\right) \quad (5)$$

The strain energy release rate, G, is computed using the average tensile force resultant, N_x, at failure of the 8-ply (n=1) laminate for each value of θ. The force resultant to cause failure of the thicker laminates (n increasing) is predicted by rearranging Equation 3 as:

$$N_x(n) = \sqrt{2hG\left(\frac{1}{(N-n)E_{LD}} - \frac{1}{NE_{LAM}}\right)^{-1}} \quad (6)$$

4. Results

In the following subsections the various forms of damage development are described, and related to the constraint ply angle and laminate size (scale factor, n). Damage due to residual thermal stress is the topic of Section 4.1. The obvious differences in the stress-strain response as a function of laminate size and constraint ply angle are presented in Section 4.2. In Section 4.3, transverse matrix cracking and first-ply failure data, as a function of constraint and size, was modeled. In Section 4.4, the development of damage after first-ply failure, as affected by the constraint ply angle and laminate size was examined with the aid of detailed x-ray and edge photomicrographs. In Section 4.5, the elastic/plastic-like stress-strain response of the $[(+60/-60/90_2)_2]_S$ lay-up was examined specifically because its response was highly sensitive to the effect of dense localized cracking not accounted for in most models available. In Section 4.6, the strength-controlling delamination of +θ° plies was predicted. The delamination of the midplane, along the -θ/90 interface, which had a strong effect on stiffness, was not examined. This decision was made because the relationship between delamination initiation and growth, for ply-level scaling of a quasi-isotropic lay-up, was successfully modeled by O'Brien (1993).

4.1. THERMAL STRESS-INDUCED MATRIX CRACKING

Thermal stress-induced cracking appeared spontaneously in the $[+\theta_n/-\theta_n/90_{2n}]_s$ laminates having high constraint (low θ angle), and thick blocks of plies (n increasing). The cracks in the

90° and +θ° or -θ° plies existed throughout the panel. It was likely that these cracks formed during cooling of the laminate from cure, though they may have formed when the first edge of the panel was trimmed. It was certain that they were not a result of cutting individual specimens, as was verified by marking the location of each crack on each specimen and piecing the panels together again to see that cracks were continuous from one specimen to the next. A summary of the thermal stress-induced crack density in the 90° plies of each $[+\theta_n/-\theta_n/90_{2n}]_s$ laminate is given in Table 3. In the columns labeled "r" the crack spacing *a* is divided by the thickness, *d*, of the 90° ply block. For +θ° ply cracking, the crack count along the length of the specimen at the top and bottom surface plies is given in Table 4.

The n=1 size laminates had no thermal stress-induced matrix cracks, nor were there cracks in any lay-up having +60° or +75° constraint plies. The n=2, 3, and 4 size lay-ups had 90° cracks, for constraint ply angles of θ = 0°, +15°, +30°, or +45°. For the n=3 size lay-up, additional cracking appeared in the top surface plies for θ = +15° and +30°. The n=4 size lay-up also had cracks in the top surface plies for θ = +45°. There was a tendency toward large numbers of cracks in the top surface plies, but few in the bottom surface plies. Finally, all of the coupon specimens had a small concave down curvature, as measured between the middle of the coupon and a flat surface. The consistent appearance, in all 24 composite panels, of convex curvature toward the underside of each coupon, indicated unbalanced resin content of the upper and lower surfaces, rather than error in orienting the plies during the hand lay-up. This phenomenon was expected from the fabrication process, because the laminate was cured against a caul plate, which is impenetrable to fluids, while excess resin was bled through the bleeder ply at the top. The warpage due to the fabrication process was studied by Radford (1993). He measured the fiber volume fraction across the thickness, and found that resin content was fairly uniform throughout the laminate thickness, but rose sharply in the ply against the caul plate, and dropped sharply in the ply against the bleeder cloth. The resin content gradient was likely responsible for the different crack counts of the +θ° ply groupings at the top and bottom surfaces.

The angle, θ, of the constraint plies relative to the 90° plies, and also the angle of the constraint plies to each other, affected whether or not stitch-like cracks formed in the -θ° plies. An x-ray of a $[+15_4/-15_4/90_8]_s$ laminate appears in Figure 1, and shows the presence of -15° stitch cracks due to a neighboring +15° crack. Constraint ply angles of 30° resulted in very few stitch cracks, but -30° cracks were much longer, see Figure 2. In Figure 3, there is a return of stitch crack formation, but now in the -45° plies due to a 90° matrix crack.

4.2. MECHANICAL TESTING: STRESS-STRAIN RESPONSE

Six representative plots of the stress-strain response of $[+\theta_n/-\theta_n/90_{2n}]_s$ laminates, for θ=0°, 15°, 30°, 45°, 60°, and 75°, appears in Figure 4. Each plot contains four curves, one for each size tested, n=1,2,3, and 4. The initial elastic modulus, strength, and strain to failure was given in Table 2. There was no size effect on the initial elastic modulus. However, it was clear that upon tensile loading, differences in damage onset stress, and development rate, resulted in early loss of stiffness, and strength, as size, n, was increased. For θ=0°, 15°, 60°, and 75°, the most obvious effect was a reduction in strength. The lay-ups having constraint plies at 30° and 45° had substantial change in the stiffness, due to midplane delamination.

4.3. FIRST-PLY FAILURE: EFFECTS OF CONSTRAINT AND THICKNESS

First-ply failure (fpf) was recorded for each $[+\theta_n/-\theta_n/90_{2n}]_s$ laminate for n=1 to 4, and for θ=0°, 15°, 30°, 45°, 60°, and 75°. The experimental data, along with predictions of the ECM, appear in Figure 5. The model was used to predict fpf for various levels of constraint, as indicated by the constraint ply angle, θ, and for the four different scales, as indicated by n. All predictions were based upon experimental data from the $[0_2/90_2]_s$ cross-ply lay-up. To maintain clarity, each plot contains the data and predictions for one size of laminate (marked on the plot as n=1, n=2, n=3, and n=4).

The residual stress state was unknown, because the lamina stress-relaxation response was not characterized. Therefore, an attempt was made to bound the possible predictions. The two extremes are full residual stress (no stress relaxation), represented as a solid curve; and no residual stress (full stress relaxation) represented as the dashed curve. Note that the value for strain energy release rate, G, computed by the model from the $[0_2/90_2]_s$ cross-ply data, was very different depending upon the residual stress that was input to it.

Examine first the plot labeled “n=1” in Figure 5. The experimental data suggested an immediate drop in the fpf stress as the constraint ply angle, θ, was increased, while the model predicted a gradual drop initially. The level of residual stress had little effect on the predictions. The plot “n=2”, corresponds to 16-ply laminates. The solid curve follows the data best, but underpredicts fpf of the cross-ply (which has a 0° constraint angle) more than the dashed curve. For both the “n=3” and “n=4” plots, corresponding to 24-ply and 32-ply laminates, respectively, there are similar trends: the solid curve follows the data best, but consistently underpredicts fpf stress of the cross-plies. On the other extreme, the dashed curve predicts the cross-ply’s dependence of fpf on n well, or is slightly nonconservative. For constraint angles up to 35 or 40° the prediction was highly nonconservative.

4.4. EFFECTS OF CONSTRAINT PLY ORIENTATION ON INTERLAMINAR AND INTRALAMINAR MATRIX CRACKING DUE TO TENSILE LOADING

In this section, damage development in the constrained 90° plies, the constraining -θ° plies, and the -θ/90 interface of $[+\theta_n/-\theta_n/90_{2n}]_s$ laminates is covered. It was found that the type of damage sustained by the respective plies depended on the angle, θ, of the constraint plies. The thickness of the ply groupings, controlled by n, affected the stress for onset of damage, and rate of damage growth.

4.4.1. Damage Progression for Constraint Plies at ±15°

The -15° plies were not damaged due to stress redistribution around the 90° cracks. Instead, the -15/90 interface delaminated from the tips of the 90° cracks, see Figure 6. Subsequent damage to the 90° plies was in the form of inclined secondary cracks near the 90° crack, see right side of Figure 7. The inclined cracks coalesce with the 90° crack-tip delaminations to form a continuous -15/90 delamination at the edge, see left side of Figure 7. The -15/90 delamination progressed deeply into the laminate, running preferentially along the 90° crack, see the magnified portion of the x-ray in Figure 8. Edge delamination was also evident, but did not penetrate with the same readiness as for constraint plies at ±30°.

4.4.2. Damage Progression for Constraint Plies at ±30°

The progression of damage was similar to that of the laminates having ±15° plies just described. After formation of 90° cracks, there was delamination of the -30/90 interface, starting from the tips of the 90° cracks, see Figure 9. Additional damage to the 90° plies appeared as inclined secondary cracks near the 90° crack, also Figure 9. The 90° crack-tip delamination penetrated deeply into the laminate interior, though 90° matrix cracks were still sparse, see Figure 10.

Only one edge of each specimen had been polished, and in this lay-up the effect was marked. The unpolished edge (right edge in Figure 11) exhibits rapid coalescence of the localized delaminations to form a continuous -30/90 delamination that penetrated from the edge toward the interior. Though polishing suppressed delamination along the left edge, it did not forestall cracking in the -30° plies, and may have encouraged it. The -30° ply cracks initiated from the tips of the 90° cracks, see magnified area of Figure 11. The -30° cracks appear fuzzy because they were inclined, as shown in Figure 12.

4.4.3. Damage Progression for Constraint Plies at ±45°

As discussed previously in Section 4.1, the appearance of 90° cracks caused stitch cracks in -45° constraint plies. When stitch cracks formed due to thermal stresses alone, little interfacial damage was found. The exception was the thickest, n=4 size, $[+45_4/-45_4/90_8]_s$ laminate. In a few instances, barely discernible -45/90 delamination along the 90° crack could be found, as shown in

the magnified portion of Figure 3. A cut was made perpendicular to the 90° crack, and the plane of the laminate, at the interior of the specimen, see Figure 13. In this highly magnified view, the -45° and 90° cracks are in close proximity, but the interface is intact.

After tensile loading, both the n=3 and n=4 sizes of laminates had clearly developed the -45/90 interfacial delamination, look ahead to Figure 22. For the n=1 and n=2 sizes, no delaminations had formed at the tips of the 90° cracks either from thermal residual stresses or after loading to failure. To be more certain, sections were taken from a failed n=1 size coupon perpendicular to the 90° crack, as shown in Figure 14. The -45° and 90° cracks were in close proximity, but no delamination was visible. From an n=2 size coupon loaded to failure, a section was taken parallel to the 90° crack, with the crack just under the polished surface, see Figure 15. An inclined -45° crack was visible, which ran across the two ply thickness up to the +45/-45 interface and the -45/90 interface. There was no sign of delamination at either interface.

4.4.4. Damage Progression for Constraint Plies at ±60°

For the n=1 size laminate loaded to 66 MPa, formation of 90° cracks was accompanied by stitch cracks in the -60° plies, see Figure 16. There existed -60/90 delaminations along the 90° crack. Immediately, a +60° crack formed at the intersection of the 90° crack with the edge. From Figure 17, observe that with little additional loading (68 MPa), more 90° cracks formed, which were confined to within a length of about 11 mm, or that defined by the coupon's width x Cos60°. The +60° cracks induced -60° stitch cracks. For the larger sizes, n=2, 3, and 4, the initiation of the first 90° crack triggered complete laminate failure.

4.5. DAMAGE AND THE RESPONSE OF $[(+60/-60/90_2)_2]_S$ LAY-UP

Earlier, it was shown that dense cracking occurs in the $-\theta°$ plies, due to a neighboring 90° crack, for θ values of 45° and 60°. The length and density of the cracks in the $-\theta°$ plies of several laminates is given in Table 5. Damage in the $[(+60/-60/90_2)_2]_s$ lay-up proceeded as follows. First, midplane 90° plies developed matrix cracks. These cracks induced short, densely spaced, cracks in the adjacent -60° plies. Delamination at the -60/90 interface was absent, in preference to forming the -60° cracks. A photomicrograph of the polished edge showing a 90° crack and the cracks induced in the -60° plies, appears in Figure 18(a). Second, matrix cracks form in the off-center 90° plies, accompanied by the same short, densely spaced, cracks in adjacent +60° and -60° plies, see Figure 18(b). As the laminate strain was increased, +60° cracks appear in the surface plies. The profusion of cracks can be seen in the x-ray of Figure 19.

Actual and modeled stress-strain responses are shown in Figure 20. The stages at which damage initiates in the various plies are indicated. The model predicts a four stage stress-strain response, as indicated by the solid line. There was the crack-free linear-elastic stage, then cracking

began first in the midplane 90° plies, next in off-center 90° plies, and lastly in all 60° plies. The actual response was similar to a linear-elastic/ perfectly plastic response.

There were three stages to the experimental stress-strain response, shown as the dashed curve in Figure 20. After the initial linear-elastic stage, the onset of cracking in the midplane 90° plies was accompanied by cracking in neighboring -60° plies. Next, cracking in the off-center 90° plies was accompanied by cracking in neighboring +60° and -60° plies. Lastly, ply scissoring at nearly 1.5% strain causes stiffening of the laminate.

4.6. DELAMINATION OF SURFACE +θ° PLIES AND PREDICTION OF STRENGTH

Ultimate strength of the $[+\theta_n/-\theta_n/90_{2n}]_s$ laminate class was controlled by the initiation of a local delamination of the surface $+\theta_n$ block of plies at the free edge, from a +θ° matrix crack. Typically, the +θ° delamination grew catastrophically when θ=15°, 30°, 60°, and 75°. For θ=45°, growth of the delamination often arrested. If delamination growth was not catastrophic, it was certainly very close to the ultimate strength. The +15° local delamination, for a $[+15/-15/90_2]_s$ laminate, was captured because of its proximity to the grip, and is shown in the x-ray of Figure 21(a). The damage sequence was 90° matrix cracking first, then a +15° matrix crack, immediately followed by -15° stitch cracking, and the initiation of the local delamination. In Figure 21(b) the n=3 size $[+15_3/-15_3/90_6]_s$ lay-up has two sites of +15° ply delamination from the +15° matrix crack. The $[+45_n/-45_n/90_{2n}]_s$ laminate class could develop several +45° surface delaminations before complete laminate failure, though they were still very close to ultimate failure, as shown in Figure 22.

In Figure 23 a photograph of the failed specimens of the size n=3, for each constraint ply angle, θ, is shown. The common characteristic of all ply angles (and sizes), is the delamination of +θ° plies from the -θ° plies. In consequence, it was possible to predict the critical load to cause failure of each.

The strength of each $[+\theta_n/-\theta_n/90_{2n}]_s$ laminate for n>1 was predicted from the strain energy release rate, G=G(θ, n=1), of the n=1 size laminate, for θ=15°, 30°, 45°, 60°, and 75°. The needed values for E_{LAM}, the modulus of the laminate, and E_{LD}, the modulus of the locally delaminated region, were computed from the lamina elastic properties using classical lamination theory, and are tabulated in Table 6. Corresponding values for G(θ, n=1) were computed using the average ultimate force resultant, N_x, of the n=1 size specimens, and Equation 3, and are shown in Table 6. The force resultant, N_x, to initiate a +θ° delamination in the n=2, 3, and 4 size laminates was predicted using the corresponding G value, and Equation 6. The results are given in Table 7, and include the percent error between the predicted and measured values. Plots of the experimental data along with the predictions are given in Figure 24. In most cases, the data scatter was greater than the error between the average experimental value and the prediction. Agreement

between the data and the model was quite good for all, with the exception of the $[+75_n/-75_n/90_{2n}]_s$ lay-up, which failed upon initiation of a 90° crack.

5. Discussion

5.1. FIRST-PLY FAILURE

In Figure 5, the equivalent constraint model was used to predict the first-ply failure of the laminates from sizes of n=2,3, and 4, and gradations of constraint from θ=0°, 15°, 30°, 45°, 60°, and 75° in the $[+\theta_n/-\theta_n/90_{2n}]_s$ layups, based on the first-ply failure stress of the $[0_2/90_2]_s$ cross-ply (n=1 size). Necessarily, the model was tuned to the material's strain energy release rate, G. Clearly, the model has captured the essence of the mechanics of first ply failure as affected by both scaling and constraint.

A problem that appeared while using this model was that it could give unexpectedly high values for G. Specifically, when the residual stress was assumed to be zero, the computed G was 250 J/m^2, a value that is within the range generally reported for graphite/epoxies, see O'Brien (1997), and was close to that reported by Bradley and Cohen (1985) for the same material. When the residual stress was at a maximum (or -138°C, the difference between fabrication and use temperatures) the computed G was 675 J/m^2, well above anything reported for carbon/epoxy, see O'Brien (1997). Thus, when stress relaxation was manipulated using the model, a large effect on fpf was predicted. Perhaps stress relaxation is the change that affects the load at which cracking will initiate. An observation that suggests the importance of stress relaxation in determining the mechanical load to initiate cracking follows.

Laminates with cracks due to thermal residual stress do not immediately resume cracking when loaded mechanically. For example, the n=3 size cross-ply cracks at about 225 MPa, which is more than 50% of the stress to cause cracking in the n=1 size. This is a lot of stress considering that the expectation is to resume cracking immediately upon application of tensile mechanical load. Moore and Dillard (1990) showed that matrix cracking appears during long-term tensile loading of cross-ply laminates. Their work shows that time-dependent change in the ability of the matrix to support load causes delayed appearance of matrix cracking. Their work lends support to the argument that a laminate containing residual fabrication stresses will also experience time-dependent changes in the matrix. It appears that to test the model more rigorously, the stress relaxation behavior of the lamina should be determined as part of a complete materials characterization process, which would include the usual measurements of elastic properties, as well as thermal and moisture expansion coefficients.

5.2. "STITCH" CRACK FORMATION

The cracks in the -θ° ply block which formed because of stress redistribution around a 90° crack were called "stitch" cracks because their length and proximity to each other resembled a stitched incision. Stitch cracks appeared in the -θ° plies due to 90° cracks when θ=-45°, see Figure 3, and in -60° plies after monotonic loading, see Figure 16. Stitch cracks were not observed in laminates having constraint ply angles at ±75°, probably because total laminate failure always occurred upon initiation of the first 90° crack. The -15° stitch cracks followed the cracks in +15° plies, not 90° plies, see Figure 1. When the constraint plies were oriented at ±30° then stitch cracks did not appear, except for a very few, see Figure 2. Tensile loading did not appear to increase the stitch crack density or change their length, see Table 5.

Stitch cracks were first described by Jamison, Schulte, Reifsnider, and Stinchcomb (1984). They considered a 1 mm thick $[0/90/+45/-45]_s$ laminate which apparently did not develop these cracks until after 50,000 tension-tension fatigue cycles at 62% of ultimate tensile load. In the present work, stitch cracks appeared due to thermal stresses, or after monotonic tensile loading. The existence of stitch cracking suggests an additional damage mechanism resulting from stress redistribution around cracks. The local delamination mechanism reported in the literature is more familiar, probably because the laminates studied were cross-plied, where constraint plies are oriented at 0° to the load direction.

In two previous studies, stitch cracks likely existed, but were overlooked. Flaggs and Kural (1982) considered T300/934 (a material having similar elastic and thermal properties to AS4/3502), with stacking sequences of $[\pm 30/90_n]_s$ and $[\pm 60/90_n]_s$, where n=1,2,4, and 8. Dye penetrant enhanced x-radiography had been used, but stitch cracks in -60° plies were not reported. Kistner, Whitney, and Browning (1985) considered AS4/3502 having stacking sequences of

$$\left[+\theta/-\theta/+\theta/-\theta/90_3/\overline{90}\right]_s, \text{ and } \left[+\theta/90/-\theta/90/+\theta/90/-\theta/\overline{90}\right]_s,$$

where θ=45° and θ=60°. Because x-radiographs were not taken, the stitch cracking was missed. In the current work, even when x-radiographs were made, the stitch cracks were fine enough that they were not visible unless the film resolution was sufficiently high. Stitch cracks were overlooked when both the fast Polaroid Type 52 (ISO 400), and finer grain Type 55 (ISO 50) films were used. Finely detailed x-radiographs were made using Kodak Industrex SR5, or Industrex M5. The development of the stitch cracks has been shown to occur in all thicknesses tested, and only required the presence of a matrix microcrack in the neighboring ply. Furthermore, the stitch cracks appeared in great numbers in plies oriented by as much as 45° from the cracked 90° ply, but were few in number for the 30° plies (oriented 60° from the cracked 90° ply). Stitch cracks are a damage form which can appear early in the service life, if not immediately after fabrication, and as such should be considered during design. State-of-the-art models can design to

avoid matrix cracking and subsequent crack-tip delamination (see Wang and Karihaloo, 1996a,b) but stitch cracks are not yet considered.

5.3. STRESS-STRAIN RESPONSE OF THE $[(+60/-60/90_2)_2]_s$ LAY-UP

The same plastic-like stress-strain response observed in the $[(+60/-60/90_2)_2]_s$ lay-up, Figure 20, was observed earlier by Kistner, Whitney, and Browning (1985) in their tests of a similar lay-up. The plastic-like stress-strain response was explained from observation (by edge inspection) that cracks appeared in all plies simultaneously. However, without high resolution x-radiographs it would not have been clear that the cracks in the interior +60° and -60° plies were actually short and stitch-like, and not cracks that ran across the laminate. Talreja (1985b) commented that the elastic/plastic-like response was expected of laminates having transverse plies with low constraint. The immediate effect of the stitch crack was to radically reduce the stiffness. Certainly, structural lay-ups will have plies oriented in the major loading directions, so the effect may not be very noticeable. However, shear stiffness may be more strongly affected.

5.4. STRENGTH OF $[+\theta_n/-\theta_n/90_{2n}]_s$ LAMINATES

The tensile strength of the $[+\theta_n/-\theta_n/90_{2n}]_s$ family of scaled angle-ply laminates was found to closely coincide with initiation of a local delamination in the $+\theta°$ plies, see Figure 24. Because of this fact, the dependence of laminate tensile strength on size was predicted successfully using O'Brien's 1993 model for predicting local delamination of this type. Damage in the form of matrix cracks and -θ/90 delamination served as favored soft zones for initiation of the $+\theta°$ crack and critical strength-controlling $+\theta°$ delamination. This is overlooked when using the model, because the modulus, E_{LAM}, of an undamaged laminate was used. Perhaps the G value computed from the n=1 size experiments is compensating for the fact that the laminate is actually locally softer than E_{LAM} suggests.

6. Conclusions

The scaling effect observed for first-ply failure of 90° plies, in $[+\theta_n/-\theta_n/90_{2n}]_s$ laminates having varying levels of constraint and varying ply thickness, has been shown to follow that predicted by a mechanics-based model. The cause for deviation of the model from the experiment may lay with the model, but certainly contributing factors must be the pre-existence of cracks in thicker laminates with high constraint, and the unknown level of residual stress.

The laminate strength was controlled by delamination of the surface $+\theta°$ ply block in the presence of a $+\theta°$ crack. Damage development before final failure, particularly the midplane delamination of layups with 30° constraint plies, governed the location of final failure. Even so,

the strength scaling effect could be predicted by use of a model customized for the $+\theta°$ ply block delamination just described.

The formation of dense numbers of short, stitch-like cracks in constraint plies of various orientation, but separated by as much as 45°, was found to occur under monotonic tensile loading or thermal stress, not only after high cycle fatigue. Furthermore, this damage mode was shown to be the cause of enormous stiffness loss in the $[(+60/-60/90_2)_2]_S$ lay-up, and not extension of long cracks in the interior +60° and -60° plies.

7. References

Aveston, J., and Kelly, A. (1973). Theory of Multiple Fracture of Fibrous Composites. Journal of Materials Science, Vol. 8, pp. 352.

Bradley, W.L. and Cohen, R.N. (1985). Matrix Deformation and Fracture in Graphite Reinforced Epoxies. In Delamination and Debonding of Materials, ASTM STP 876, October, pp. 389-410.

Crossman, F. W., and Wang, A.S.D. (1982). The Dependence of Transverse Cracking and Delamination on Ply-Thickness in Graphite/Epoxy Laminates. American Society for Testing and Materials.

Curtis, P.T. (1980). The Effect of Edge Stresses on the Failure of (0°,45°,90°) CFRP Laminates. Royal Aircraft Establishment Technical Report TR 80054.

Dvorak, G.J., and Laws, N. (1987). Analysis of Progressive Matrix Cracking in Composite Laminates II. First Ply Failure. Journal of Composite Materials, Vol. 21, April, pp. 309-329.

Flaggs, D.L., and Kural, M.H. (1982). Experimental Determination of the In Situ Transverse Lamina Strength in Graphite/Epoxy Laminates. Journal of Composite Materials, Vol. 16, March, pp. 103-116.

Fukunaga, H., Chou, T.-W., Schulte, K., Peters, P. W. M. (1984). Probabilistic Initial Failure Strength Of Hybrid And Non Hybrid Laminates. Journal of Materials Science, Vol. 19, No.11, pp. 3546-3553.

Gudmundson, P., Östlund, S., and Zang, W. (1992). Local Stresses and Thermoelastic Properties of Composite Laminates Containing Micro Cracks. Local Mechanics Concepts for Composite Material Systems (edited by J.N. Reddy and K.L. Reifsnider), Springer, Berlin, pp. 283-308.

Gudmundson, P., and Zang, W. (1993). An Analytic Model for Thermoelastic Properties of Composite Laminates Containing Transverse Matrix Cracks. International Journal of Solids and Structures, Vol. 30, No. 23, pp. 3211-3231.

Hashin, Z. (1985). Analysis of Cracked Laminates: A Variational Approach. Mechanics of Materials, Vol. 4, pp. 121-136.

Herakovich, C.T. (1981). On the Relationship Between Engineering Properties and Delamination of Composite Materials. Journal of Composite Materials, Vol. 15, pp. 336-348.

Herakovich, C.T. (1982). Influence of Layer Thickness on the Strength of Angle-Ply Laminates. Journal of Composite Materials, Vol. 16, May, pp. 216-227.

Herakovich, C.T., Post, D., Buczek, M.B., Czarnek, R. (1985). Free Edge Strain Concentrations in Real Composite Laminates: Experimental-Theoretical Correlation. Journal of Applied Mechanics, Vol. 52, No. 4, pp. 787-793.

Highsmith, A.L. and Reifsnider, K.L. (1982). Stiffness-Reduction Mechanisms in Composite Laminates. Damage in Composite Materials, ASTM STP 775, K.L. Reifsnider, Ed., American Society for Testing and Materials, pp. 103-117.

Hsu, P. W. and Herakovich., C.T. (1977). Edge Effects in Angle-Ply Composite Laminates. Journal of Composite Materials, Vol. 11, pp. 422-428.

Jackson, K.E., and Kellas, S. (1993). Effect of Specimen Size on the Tensile Strength of Geometrically Scaled $[+\theta_n/-\theta_n/90_{2n}]_s$ Composite Laminates. Army Symposium on Solid Mechanics, August 17-19, Plymouth, MA.

Jamison, R.D., Schulte, K., Reifsnider, K.L., and Stinchcomb, W.W. (1984). Characterization and Analysis of Damage Mechanisms in Tension-Tension Fatigue of Graphite/Epoxy Laminates. Effects of Defects in Composite Materials, ASTM STP 836, American Society for Testing and Materials, Philadelphia, pp. 21-55.

Kellas, S., and Morton, J. (1990). Strength Scaling in Fiber Composites. NASA Contractor Report 4335, November.

Kellas, S., and Morton, J. (1992). Scaling Effects in Angle-Ply Laminates. NASA Contractor Report 4423, February.

Kellas, S., Johnson, D.P., Morton, J., and Jackson, K.E. (1993). Scaling Effects in Sublaminate-Scaled Composite Laminates. 34th AIAA/ASME/ASCE/AHS/ASC Structures, Structural Dynamics and Materials Conference, AIAA/ASME Adaptive Structures Forum, April 19-22, La Jolla, CA, Part 6, pp. 3715-3725.

Kim, R. Y., Soni, S.R. (1984). Experimental and Analytical Studies On the Onset of Delamination in Laminated Composites. Journal of Composite Materials, Vol. 18, pp. 70-80.

Kistner, M.D., Whitney, J.M., and Browning, C.E. (1985). First-Ply Failure of Graphite/Epoxy Laminates. Recent Advances in Composites in the United States and Japan, ASTM STP 864, J.R. Vinson and M. Taya, Eds., American Society for Testing and Materials, Philadelphia, pp. 44-61.

Lagace, P., Brewer, J., and Kassapoglou, C. (1987). The Effect of Thickness on Interlaminar Stresses and Delamination in Straight-Edged Laminates. Journal of Composites Technology and Research, JCTRER, Vol. 9, No. 3, pp. 81-87.

Moore, R.H., and Dillard, D.A. (1990). Time-dependent Matrix Cracking in Cross-ply Laminates. Composites Science and Technology, Vol. 39, pp. 1-12.

O'Brien, T.K. (1982a). The Effect of Delamination on the Tensile Strength of Unnotched, Quasi-Isotropic, Graphite/Epoxy Laminates. Proceedings of the 1982 Joint Conference on Experimental Mechanics, Oahu-Maui, Hawaii, May 23-28, pp. 236-243.

O'Brien, T. K. (1982b). Characterization of Delamination Onset and Growth in a Composite Laminate. Damage in Composite Materials, ASTM STP 775, American Society for Testing and Materials, Philadelphia, pp. 140-167.

O'Brien, T.K., and Salpekar, S.A. (1993). Scale Effects on the Transverse Tensile Strength of Graphite/Epoxy Composites. Composite Materials: Testing and Design (Eleventh Volume), ASTM STP 1206, E.T. Camponeschi, Jr., Ed., American Society for Testing and Materials, Philadelphia, pp. 23-52.

O'Brien, T.K., and Hooper, S.J. (1993). Local Delaminations in Laminates with Angle Ply Matrix Cracks, Part I: Tension Tests and Stress Analysis. Composite Materials: Fatigue and Fracture, Fourth Volume, ASTM STP 1156, W.W. Stinchcomb and N.E. Ashbaugh, Eds., American Society for Testing and Materials, Philadelphia, pp. 491-506.

O'Brien, T.K. (1993). Local Delaminations in Laminates with Angle Ply Matrix Cracks, Part II: Delamination Fracture Analysis and Fatigue Characterization. Composite Materials: Fatigue and Fracture, Fourth Volume, ASTM STP 1156, W.W. Stinchcomb and N.E. Ashbaugh, Eds., American Society for Testing and Materials, Philadelphia, pp. 407-538.

O'Brien, T.K. (1997). Composite Interlaminar Shear Fracture Toughness, G_{IIc}: Shear Measurement or Sheer Myth? NASA Technical Memorandum 110280, February.

Oplinger, D.W., Parker, B.S., and Chiang, F.P. (1974). Edge-Effect Studies in Fiber-Reinforced Laminates. Experimental Mechanics, Vol. 14, No. 9, pp. 347-354.

Pagano, N.J., and Pipes, R.B. (1973). Some Observations on the Interlaminar Strength of Composite Laminates. International Journal of Mechanical Sciences, Vol. 15, pp. 679-688.

Parvizi, A., Garrett, K.W., Bailey, J.E. (1978). Constrained Cracking in Glass Fibre-Reinforced Epoxy Cross-Ply Laminates. Journal of Materials Science, Vol. 13, pp. 195-201.

Pipes, R.B., and Pagano, N.J. (1970). Interlaminar Stresses in Composite Laminates Under Uniform Axial Extension. Journal of Composite Materials, Vol. 4, October, pp. 538-548.

Pipes, R.B., and Daniel, I.M. (1971). Moiré Analysis of Interlaminar Shear Edge Effect in Laminated Composites. Journal of Composite Materials, Vol. 5, pp. 255-259.

Radford, D.W. (1993). Cure Shrinkage Induced Warpage in Flat Uni-Axial Composites, Journal of Composites Technology and Research, JCTRER, Vol. 15, No. 4, pp. 290-296.

Reifsnider, K.L. (1977). Some Fundamental Aspects of the Fatigue and Fracture Response of Composite Materials. Proceedings of the 14th Annual Meeting, Society of Engineering Science, G.C. Sih, Ed., Lehigh University, Bethlehem, PA, Nov. 14-16. Recent Advances in Engineering Science, pp. 373-384.

Rodini, B.T., and Eisenmann, J.R. (1978). An Analytical and Experimental Investigation of Edge Delamination in Composite Laminates. Fibrous Composites in Structural Design. New York, Plenum Press. 441-457.

Talreja, R. (1985a). A Continuum Mechanics Characterization of Damage in Composite Materials. Proceedings of the Royal Society of London, A399, pp. 195-216.

Talreja, R. (1985b). Transverse Cracking and Stiffness Reduction in Composite Laminates. Journal of Composite Materials, Vol. 19, July, pp. 355-375.

Talreja, R. (1986). Stiffness Properties of Composite Laminates with Matrix Cracking and Interior Delaminations. Engineering Fracture Mechanics, Vol. 25, No. 5/6, pp. 751-762.

Talreja, R. (1996). A Synergistic Damage Mechanics Approach to Durability of Composite Material. Progress in Durability Analysis of Composite Systems. Cardon, Fukuda and Reifsnider, Eds. Balkema, Rotterdam, ISBN: 90 5410 809 6, pp. 117-129.

Varna, J., and Berglund, L.A. (1991). Multiple Transverse Cracking and Stiffness Reduction in Cross-Ply Laminates. Journal of Composites Technology and Research, Vol. 13, pp. 97-106.

Varna, J., Berglund, L.A., Talreja, R., and Jacovics, A. (1993). A Study of the Opening Displacement of Transverse Cracks in Cross-Ply Laminates. International Journal of Damage Mechanics, Vol. 2, pp. 272-289.

Vasil'ev, V.V., Dudchenko, and A.A., Elpat'evskii, A.N. (1970). Analysis of the Tensile Deformation of Glass-Reinforced Plastics. Mekhanika Polimerov, Vol. 1, pp. 144-147.

Wang, J., and Karihaloo, B.L. (1994). Cracked Composite Laminates Least Prone to Delamination. Proc. of the Royal Society London, Vol. 444, pp. 17-35.

Wang, J., and Karihaloo, B.L. (1996a). Optimum in Situ Strength Design of Composite Laminates Part I: In Situ Strength Parameters. Journal of Composite Materials, Vol. 30, No. 6, pp. 1314-1337.

Wang, J., and Karihaloo, B.L. (1996b). Optimum in Situ Strength Design of Composite Laminates Part II: Optimum Design. Journal of Composite Materials, Vol. 30, No. 12, pp. 1338-1358.

Zhang, J., Fan, J., and Soutis, C. (1992). Analysis of Multiple Matrix Cracking in $[\pm\theta_m/90_n]_s$ Composite Laminates, Part 2: Development of Transverse Ply Cracks. Composites, Vol. 23, No. 5, September 1992, pp. 299-304.

Zhang, J., Soutis, C., and Fan, J. (1994a). Strain Energy Release Rate Associated with Local Delaminations in Cracked Composite Laminates. Composites, Vol. 25, No. 9, pp. 851-862.

Zhang, J., Soutis, C., and Fan, J. (1994b). Effects of Matrix Cracking and Hygrothermal Stresses on the Strain Energy Release Rate for Edge Delamination in Composite Laminates. Composites, Vol. 25, No.1, pp. 27-35.

Table 1. Specimen sizes and dimensions.

scale	n	plies	length (mm)	width (mm)	thickness (mm)
1/4	1	8	146.1	12.7	1.092
1/2	2	16	292.1	25.4	2.159
3/4	3	24	438.2	38.1	3.302
Full	4	32	584.2	50.8	4.394

Table 2. Mechanical properties of $[+\theta_n/-\theta_n/90_{2n}]_s$ laminates for differing size, n.

θ	n=1			n=2			n=3			n=4		
degrees	modulus GPa	strength MPa	strain %	modulus GPa	strength MPa	strain %	modulus GPa	strength MPa	strain %	modulus GPa	strength MPa	strain %
0	74.3	843.2	1.24	71.5	814.5	1.11	70.5	796.6	1.08	73.8	764.7	1.02
15	65.5	449.6	0.726	63.3	324.7	0.541	62.6	271.9	0.446	61.0	234.5	0.393
30	42.1	270.2	0.824	–	173.2	–	41.7	156.9	0.441	40.3	139.6	0.395
45	22.5	140.5	0.843	–	84.7	–	20.8	79.4	0.577	19.7	79.3	0.503
60	13.3	65.9	0.521	12.2	53.0	0.443	12.4	44.9	0.357	12.9	33.7	0.287
75	10.9	43.9	0.417	10.2	42.6	0.513	10.4	35.7	0.334	10.2	31.1	0.303
90	10.8	39.3	0.366	10.1	38.3	0.383	10.2	38.2	0.377	10.2	37.0	0.846

Table 3. Thermal Stress Induced 90° Crack Density of $[+\theta_n/-\theta_n/90_{2n}]_s$

		constraint ply angle							
		0°		15°		30°		45°	
scale	n	$d^{(1)}$ (cm)	$r^{(2)}$	d (cm)	r	d (cm)	r	d (cm)	r
1/4	1	∞	0	∞	0	∞	0	∞	0
1/2	2	1.02	0.10	0.37	0.27	0.33	0.30	4.17	0.02
3/4	3	0.42	0.36	0.34	0.45	0.87	0.17	0.64	0.24
Full	4	0.39	0.51	0.45	0.44	1.00	0.20	0.67	0.30

(1) d is the average crack spacing in the 90° plies.
(2) r is the micro crack density, where $r=a/d$, and a = the 90° ply block thickness.

Table 4. Count of Thermal Stress-Induced Cracks in +θ° Plies

gauge length, mm	n	+θ° constraint ply angle							
		0°		15°		30°		45°	
		top	bottom	top	bottom	top	bottom	top	bottom
146.1	1	0	0	0	0	0	0	0	0
292.1	2	0	0	0	0	0	0	0	0
438.2	3	0	0	11	0	50	0	0	0
279.4	4	4	4	4	0	0	1	28	0

Table 5. Length and Density of Cracks in -θ° Plies

scale	specimen no.	θ° ply	tensile stress (MPa)	crack density[(1)] (cracks/cm)	crack length, (mm)	
					min.,max.	mean (st.dev.)
3/4	3-15-9*	-15	thermal stress	33,34,31	0.15, 1.95	0.82 (0.71)
Full	4-15-1*	-15	thermal stress	8,6,7.3,8,9.3, 7.3		
1/4	1-45-11	-45	134.7	72,62,64	0.10, 0.50	0.32 (0.11)
1/4	1-45-12	-45	140.4	60,64,60	0.10, 1.50	0.32 (0.11)
1/2	2-45-9	-45	413.4	56,58,44,50,56	0.10, 0.95	0.65 (0.22)
1/2	2-45-11	-45	thermal stress	52,48,60,52		
1/2	2-45-10	-45	406.3		0.25, 1.00	0.65 (0.19)
3/4	3-45-1	-45	thermal stress	12,6,0,0,0,2,2,3, 10	0.40, 1.50	1.13 (0.35)
3/4	3-45-11	-45	92.9	25,28,42,30	0.20, 2.00	1.12 (0.45)
Full	4-45-1	-45	thermal stress	8,9,11,16		
Full	4-45-?	-45				
1/4	1-60-9	-60	68.0	46,42,56,38	0.15, 0.50	0.35 (0.11)
1/4	1-60-11	-60	66.1	50,44,48	0.25, 0.70	0.44 (0.14)
1/2	2-60-11	-60	60.0	33,28,28	0.30, 0.90	0.58 (0.16)

* these -15° cracks follow the +15° crack

(1) The crack density includes cracks counted in both -θ° layers.

Table 6. Stiffnesses and Strain Energy Release Rate for Delamination of +θ° Plies

θ	E_{LAM} (GPa)	E_{LD} (GPa)	G (J/m^2)
15	66.3	32.2	2058
30	44.9	14.3	2110
45	24.0	5.4	1694
60	13.7	3.4	567
75	11.2	3.2	263

Table 7. Experimental results for strength of $[+\theta_n/-\theta_n/90_{2n}]_s$ laminates. Predictions are for initiation of delamination of the surface $+\theta_n$ ply block. Error numbers indicate how closely strength was controlled by the start of delamination.

θ=15° n	σ_{ult} (MPa) (experiment)	N_x (kN/m) (experiment)	N_x (kN/m) (prediction)	% error
1	449.6	449.6	--	--
2	324.7	649.6	635.8	-2.1
3	271.9	815.6	778.6	-4.5
4	234.5	938.0	899.1	-4.2

θ=30° n	σ_{ult} (MPa) (experiment)	N_x (kN/m) (experiment)	N_x (kN/m) (prediction)	% error
1	270.2	270.2	--	--
2	173.2	346.4	382.1	+10.3
3	156.9	470.7	468.0	-0.6
4	139.6	558.4	540.4	-3.2

θ=45° n	σ_{ult} (MPa) (experiment)	N_x (kN/m) (experiment)	N_x (kN/m) (prediction)	% error
1	140.5	140.5	--	--
2	84.7	169.4	198.7	+17.3
3	79.4	238.2	243.4	+2.2
4	79.3	317.2	281.0	-11.4

θ=60° n	σ_{ult} (MPa) (experiment)	N_x (kN/m) (experiment)	N_x (kN/m) (prediction)	% error
1	65.9	65.9	--	--
2	53.0	106.0	93.2	-12.1
3	44.9	134.7	114.1	-15.3
4	33.7	134.8	131.8	-2.2

θ=75° n	σ_{ult} (MPa) (experiment)	N_x (kN/m) (experiment)	N_x (kN/m) (prediction)	% error
1	43.9	43.9	--	--
2	42.6	85.2	62.0	-27.2
3	35.7	107.1	76.0	-29.0
4	31.1	124.4	87.0	-30.1

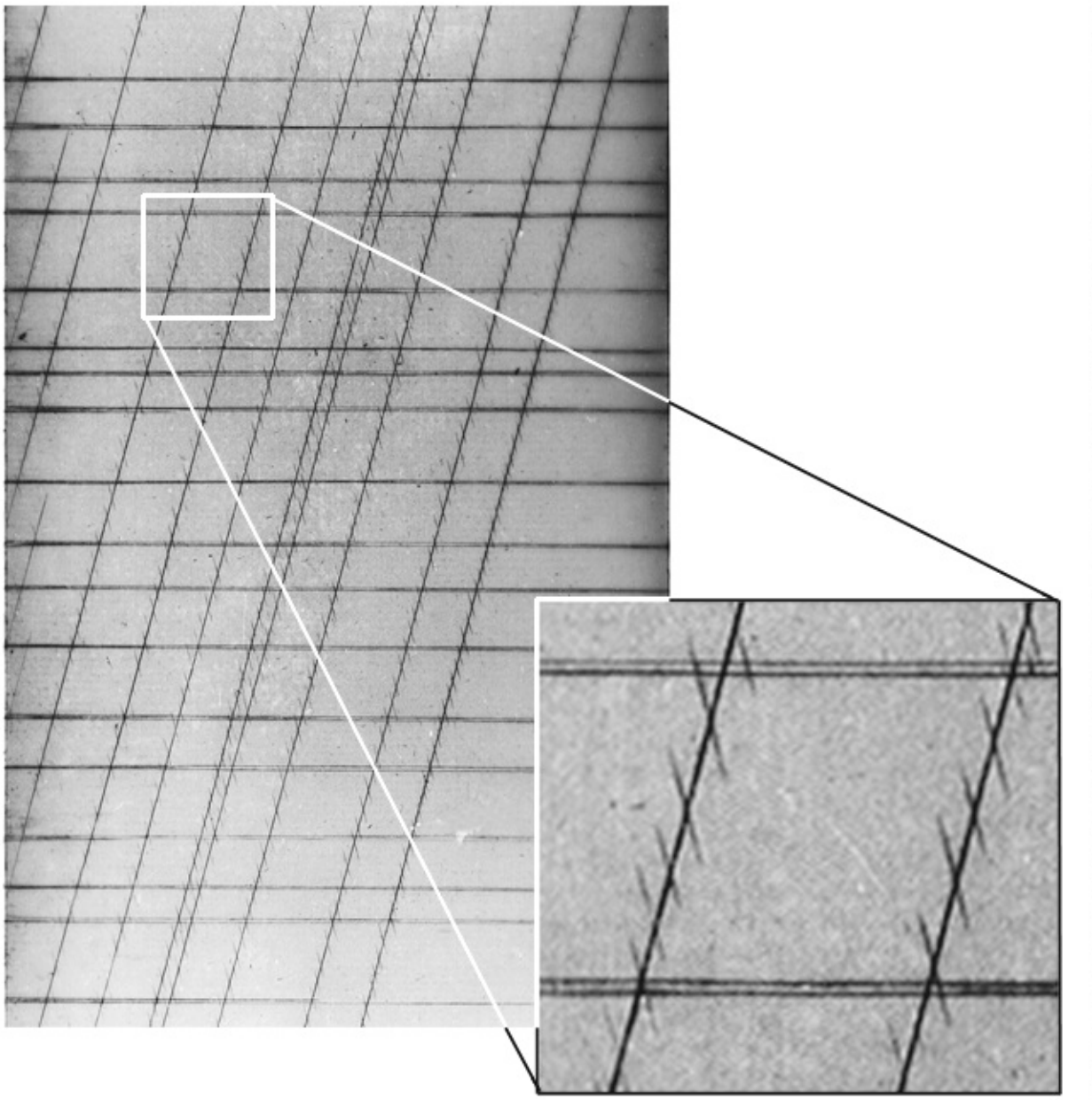

Figure 1. X-radiograph of thermal stress-induced matrix microcracks in the n=4 size layup $[+15_4/-15_4/90_8]_s$. The 90° ply matrix cracks run from left to right. Stress redistribution around the +15° ply matrix cracks induce formation of short, stich-like, -15° ply matrix cracks.

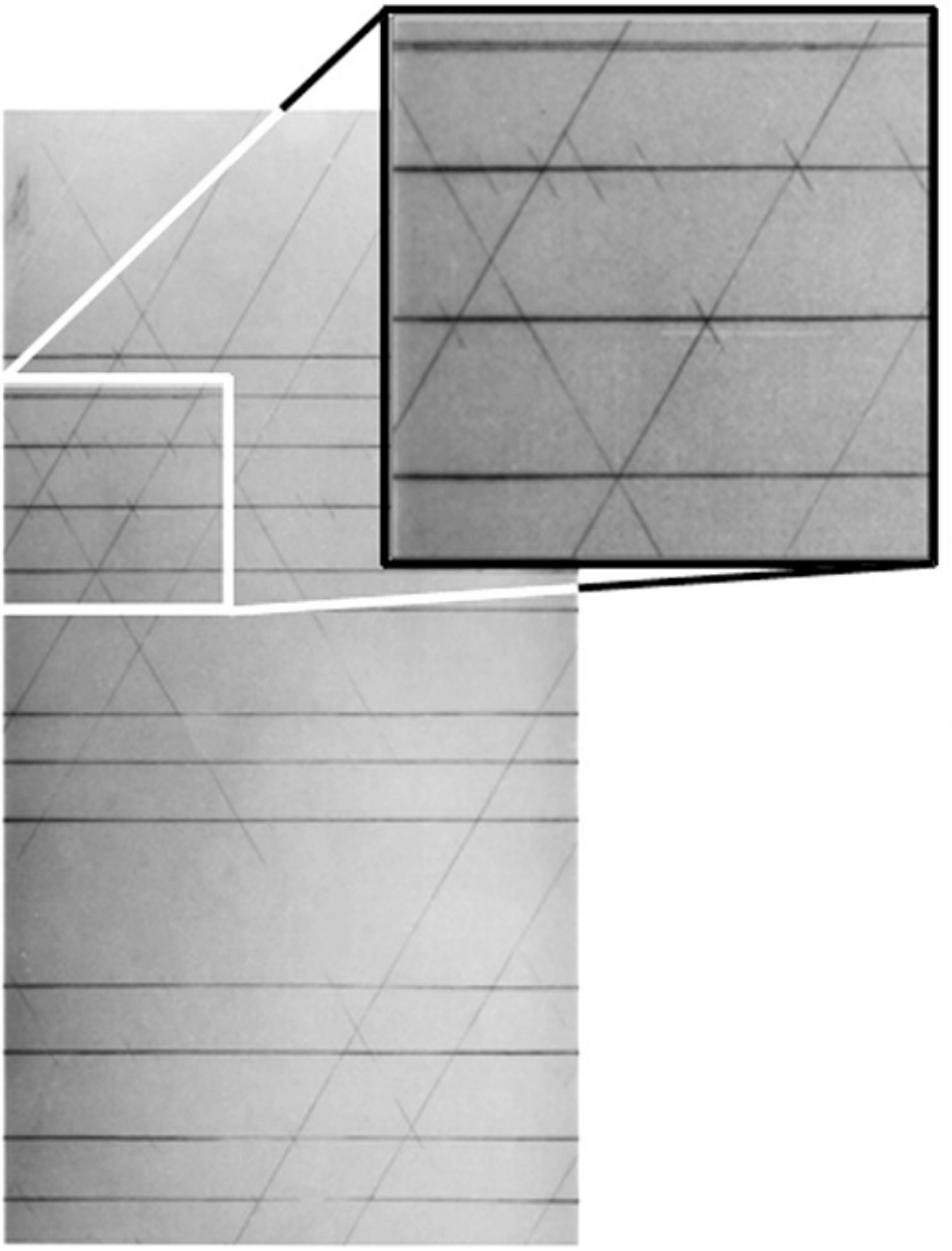

Figure 2. X-radiograph of thermal stress-induced matrix microcracks in the n=4 size layup $[+30_4/-30_4/90_8]_s$. The 90° ply matrix cracks run from left to right, and trigger formation of a few short, stich-like, -30° ply matrix cracks. This layup exhibits long -30° ply matrix cracks, in addition to +30° ply matrix cracks.

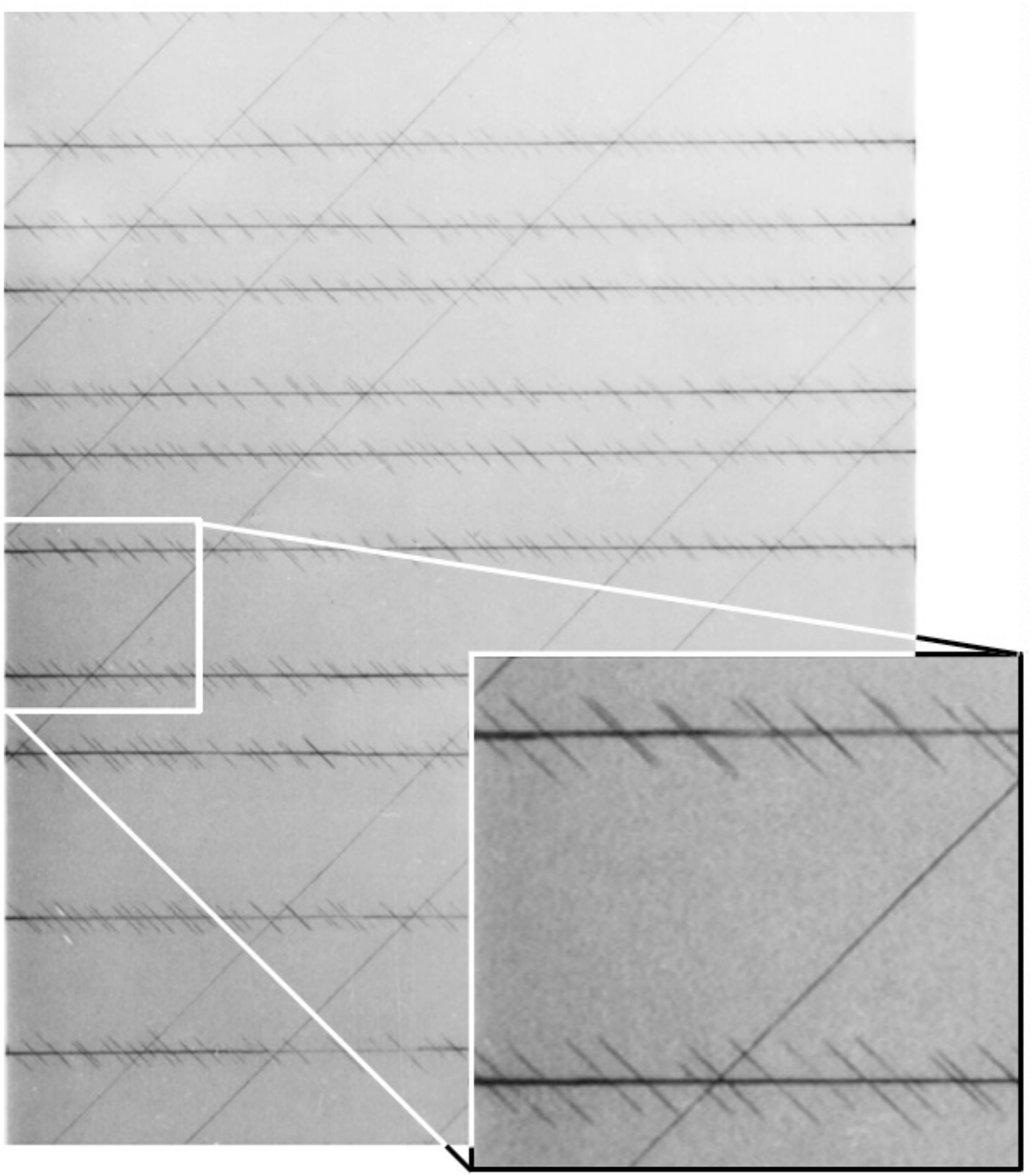

Figure 3. X-radiograph of thermal stress-induced matrix microcracks in the ply-level scaled, (n=4) layup $[+45_4/-45_4/90_8]_s$. The 90° ply matrix cracks run from left to right, and trigger formation of a many short, stich-like, -45° ply matrix cracks. Long +45° ply matrix cracks appear.

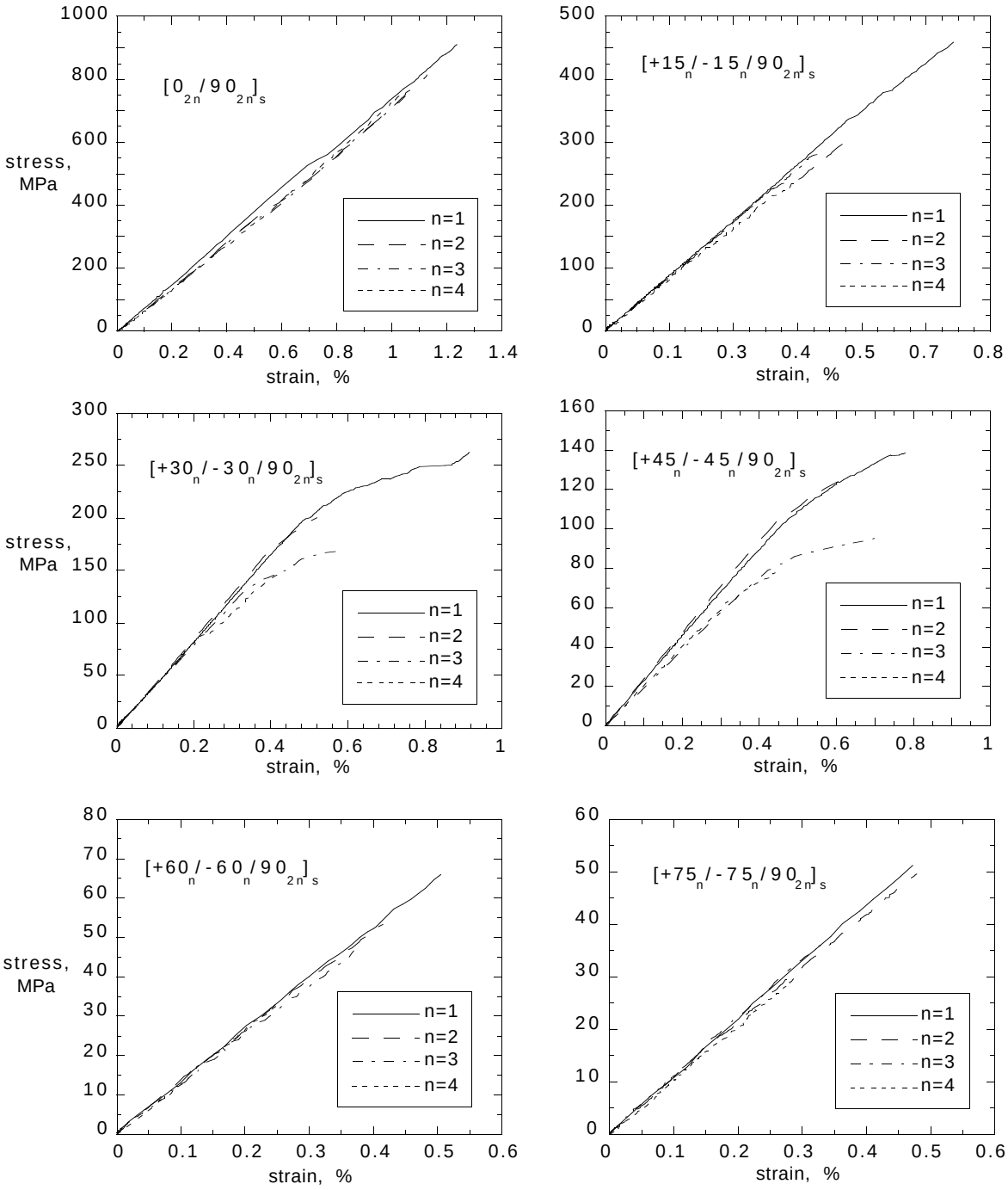

Figure 4. Typical stress versus strain plots for $[+\theta_n/-\theta_n/90_{2n}]_s$ laminates.

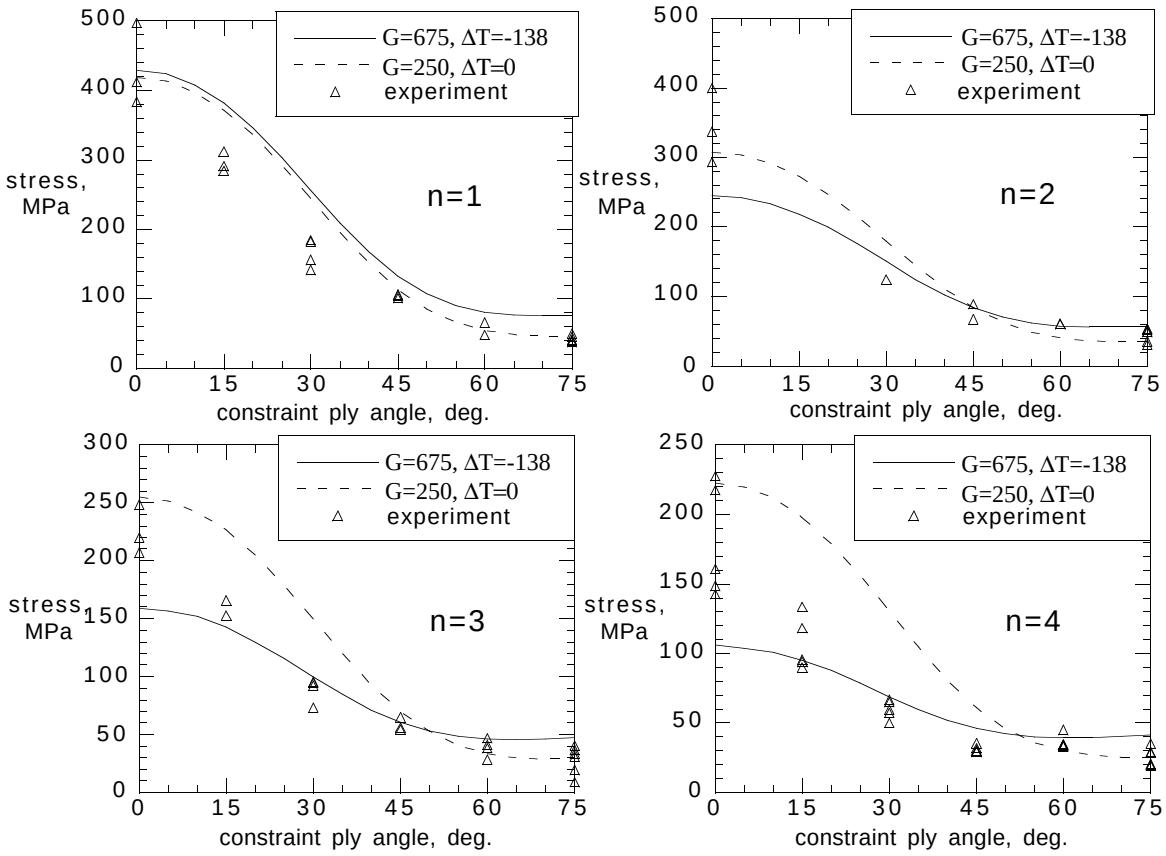

Figure 5. First-ply failure of $[+\theta_n/-\theta_n/90_{2n}]_s$ in the central block of 90° plies as a funtion of both the angle of the constraining plies, and the thickness of the laminate, as governed by *n*. The predictions are made using the "Equivalent Constraint Model" Zhang and Soutis (1992). All predictions are based upon first-ply failure tests of the $[0_2/90_2]_s$ (n=1) size cross-ply laminate. Model parameters were: G=675 J/m^2, ΔT=-138°C (solid line), and G=250 J/m^2, ΔT=0°C (dashed line).

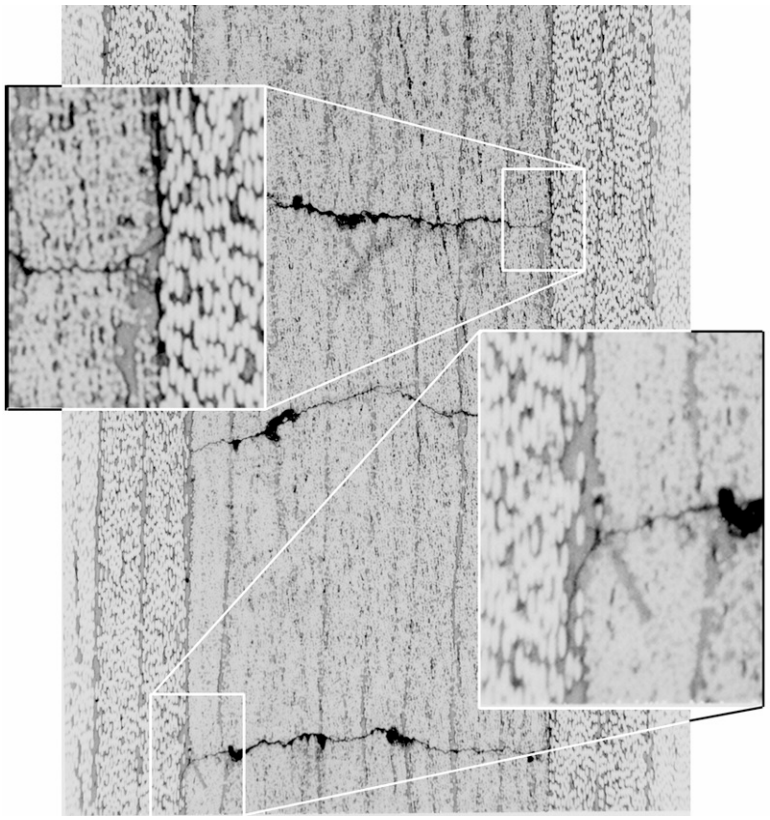

Figure 6. Development of -15/90 interface failure at 90° crack tips as a consequence of stress redistribution around the 90° cracks. Shown is a $[+15_2/-15_2/90_4]_s$ laminate, loaded to 283 MPa.

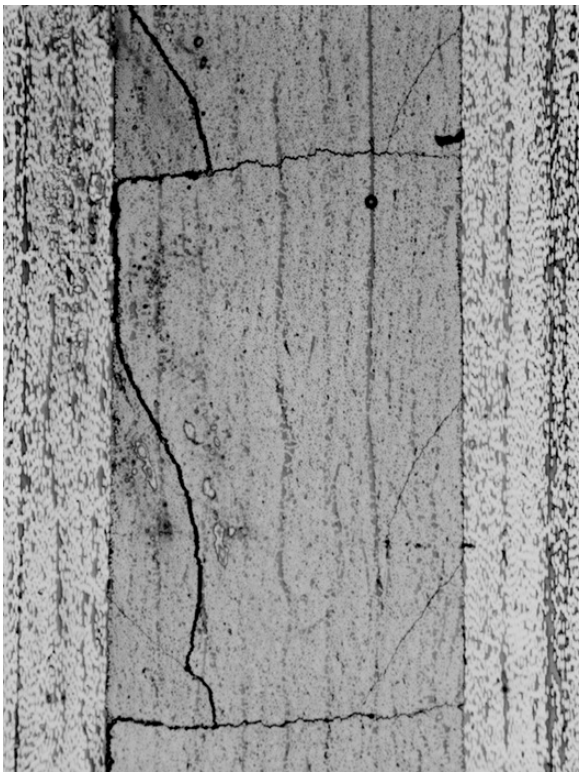

Figure 7. Coalescence of inclined secondary cracks in the 90° plies with 90° crack-tip delaminations into a continuous -15/90 interface delamination. Shown is a $[+15_2/-15_2/90_4]_s$ laminate, loaded to 339 MPa.

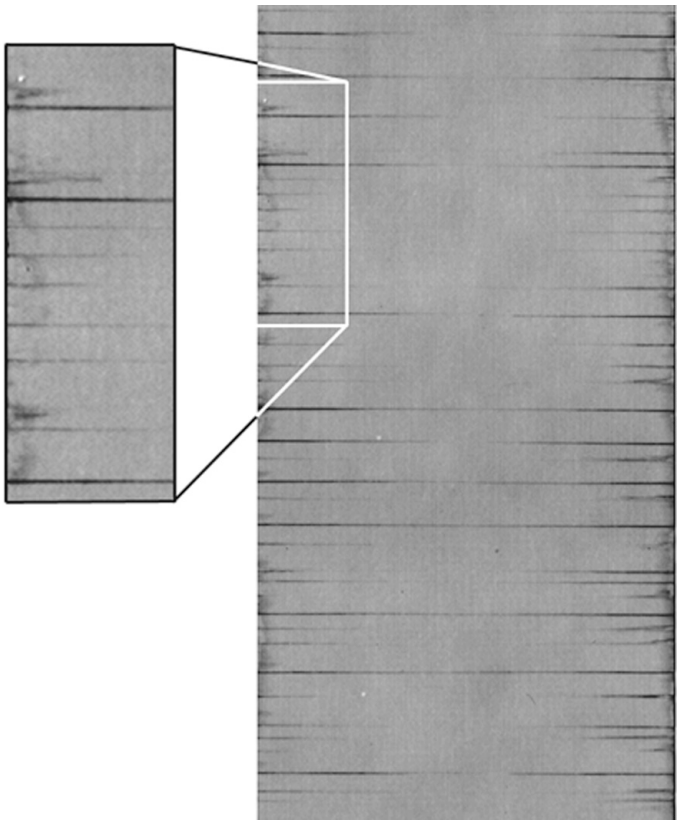

Figure 8. Comparatively high loading did not produce a general edge delamination. Delaminations were very localized and associated with 90° crack-tip delamination. Shown is a $[+15_2/-15_2/90_4]_s$ laminate, loaded to 311 MPa.

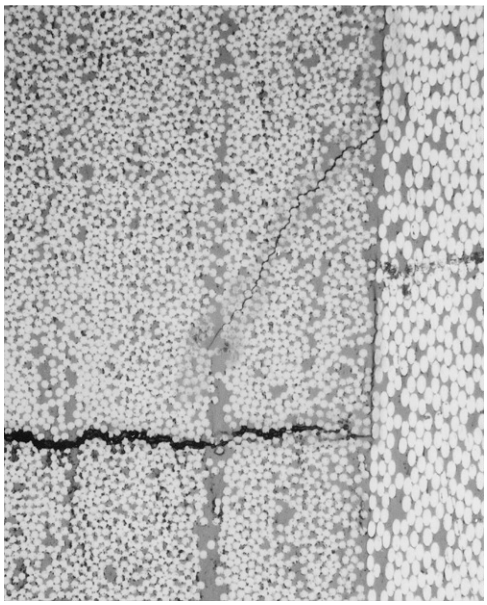

Figure 9. Development of -30/90 delamination from the tip of the 90° crack. Further development of inclined cracking in the 90° plies. Shown is a $[+30_2/-30_2/90_4]_s$ layup, loaded to 124 MPa.

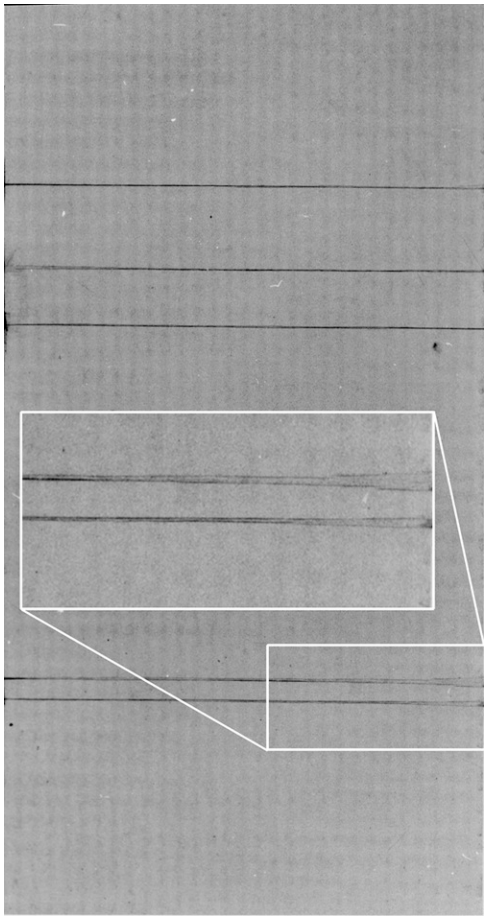

Figure 10. Delamination of the -30/90 interface from 90° crack tips ran deeply into the laminate, before 90° matrix cracking became well developed. Shown is a $[+30/-30/90_2]_s$ layup, loaded to 209 MPa.

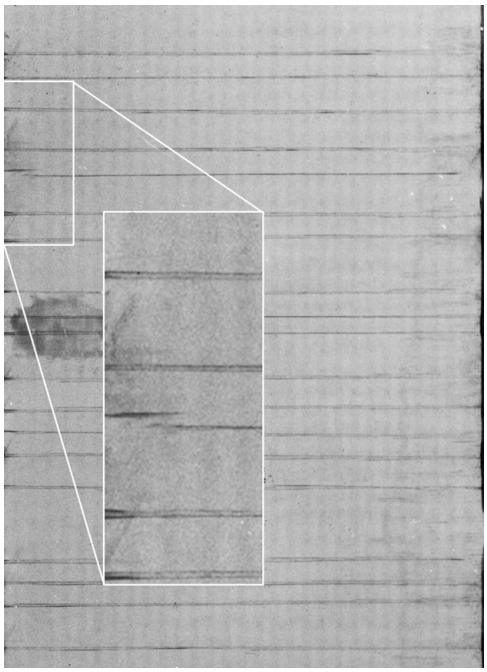

Figure 11. Progress of damage in a $[+30/-30/90_2]_s$ layup loaded to 227 MPa. Right edge, unpolished, shows rapid coalescence of -30/90 local delaminations had formed one large edge delamination. Left edge shows that polishing suppressed the edge delamination, but that -30° cracks formed instead.

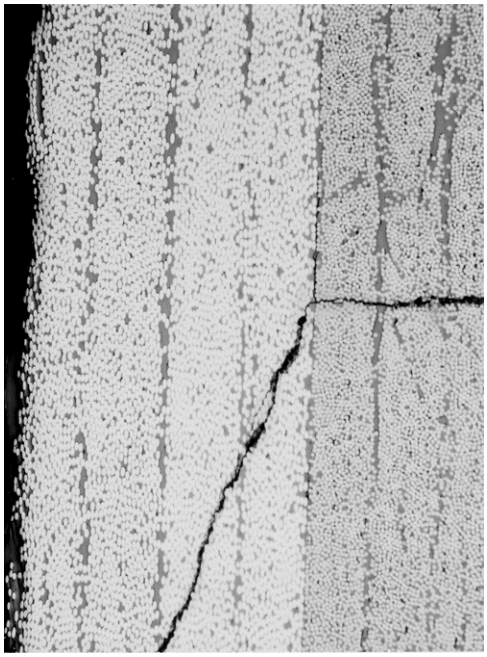

Figure 12. Growth of a -30° crack from the tip of a 90° crack at the -30/90 interface. Shown is a $[+30_2/-30_2/90_4]_s$ laminate, loaded to 160 MPa.

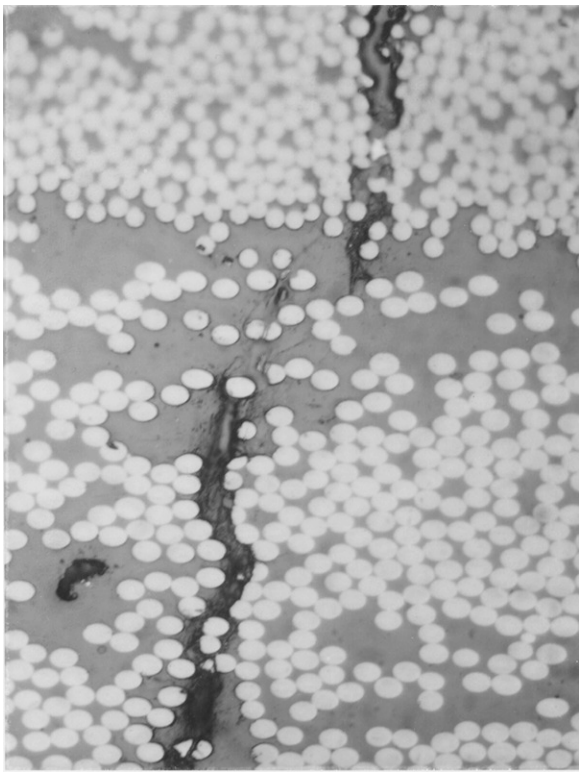

Figure 13. Internal view, perpendicular to the 90° plies, close to the intersection of a -45° stitch crack and a 90° crack. There was no -45/90 delamination. Specimen was an n=4 size, $[+45_4/-45_4/90_8]_s$ laminate, not yet loaded. Magnification is 400X.

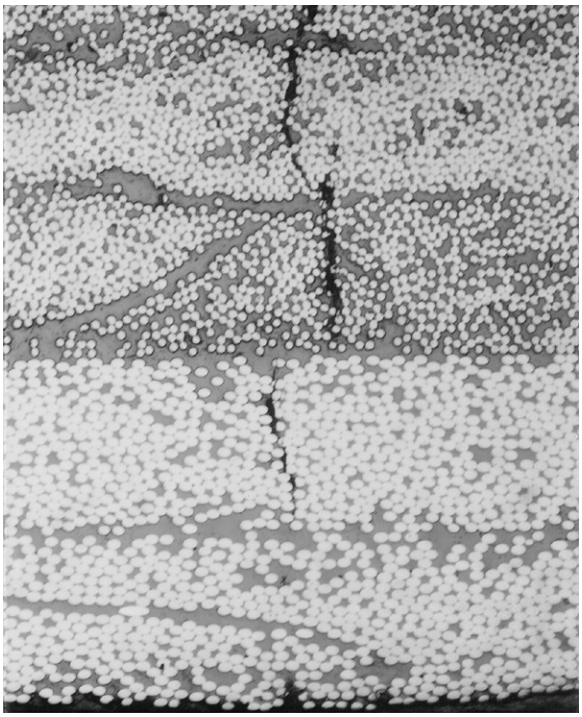

Figure 14. An interior section, close to the intersection of the -45° and 90° cracks, cut and polished perpendicular to the 90° plies. Shown is a $[+45/-45/90_2]_s$ laminate which had been loaded to failure. No -45/90 delamination can be observed.

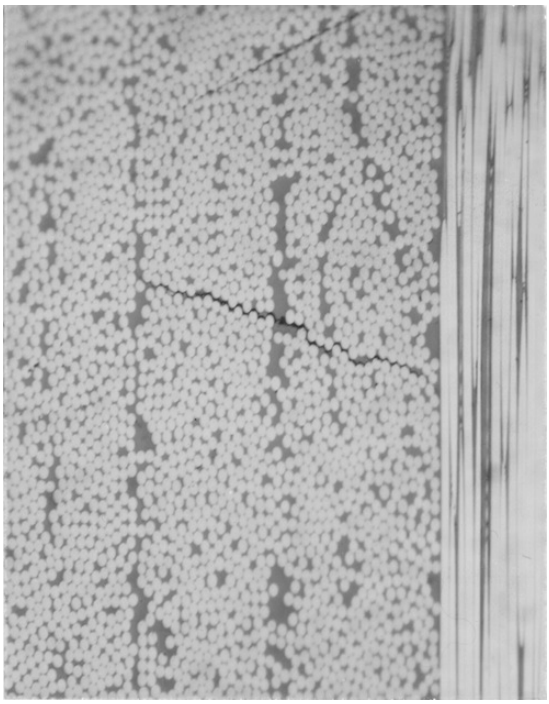

Figure 15. An interior section, cut and polished parallel to the 90° plies, and close to the 90° crack. A -45° stitch crack is evident, but -45/90 delamination cannot be seen. Specimen was a $[+45_2/-45_2/90_4]_s$ loaded to 101 MPa.

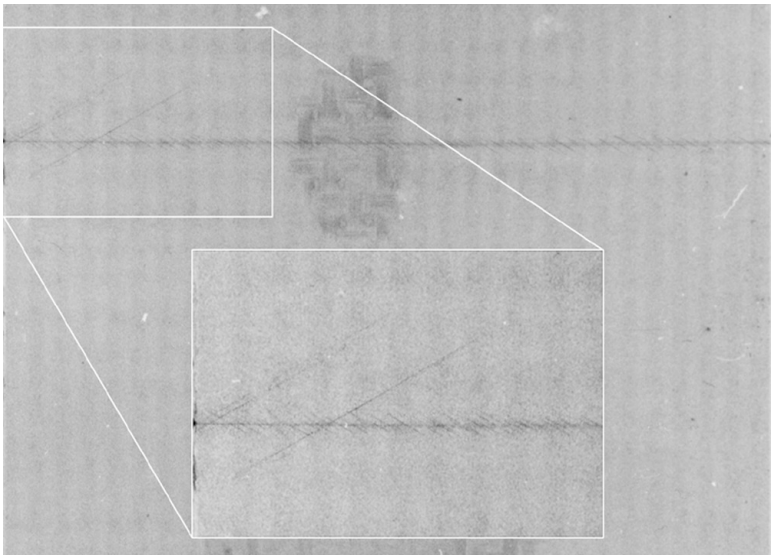

Figure 16. Formation of 90° cracks results in -60° stitch cracks. The +60° cracks initiate from -60° cracks, and prefer to start near 90° cracks. Specimen is a $[+60/-60/90_2]_s$ layup, loaded to 66 MPa.

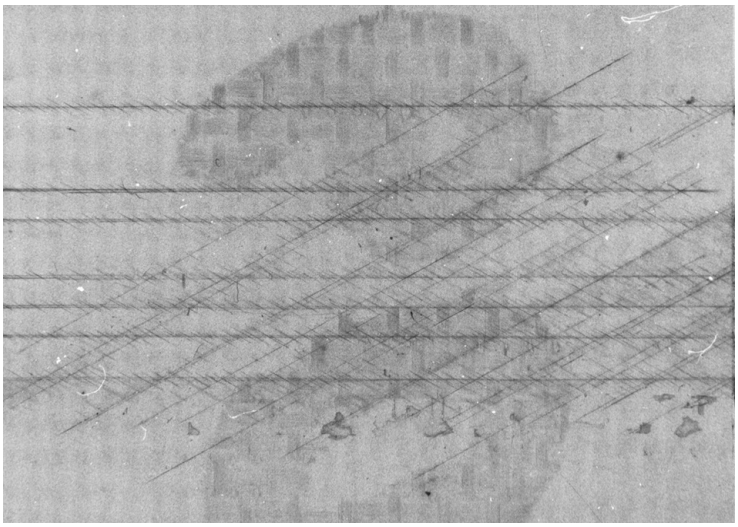

Figure 17. Additional 90° cracks formed, but under the +60° cracks. Stitch cracks in the -60° plies formed due to +60° cracks. Specimen is a $[+60/-60/90_2]_s$ layup, loaded to 68 MPa. Failure was imminent.

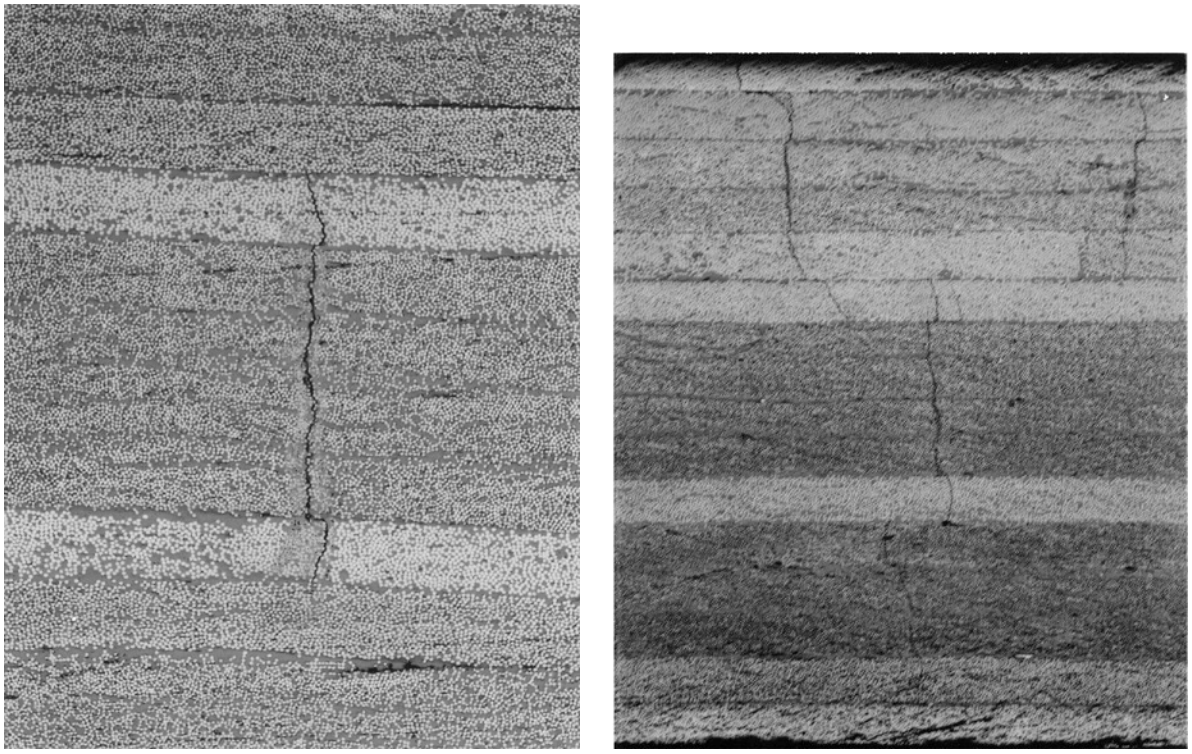

(a) first failure (b) second failure

Figure 18. Micrographs of the polished edge of the sublaminate-level scaled $[(+60/-60/90_2)_2]_s$ layup. The first failure event (a) occurs at 63 MPa, and consists of midplane 90° ply matrix cracks and immediate formation of short, stich-like, -60° ply matrix cracks. The second failure event (b) occurs at 75 MPa, and consists of off-center 90° ply matrix cracks and immediate formation of short, stich-like, -60° and +60° ply matrix cracks in all remaining 60° plies.

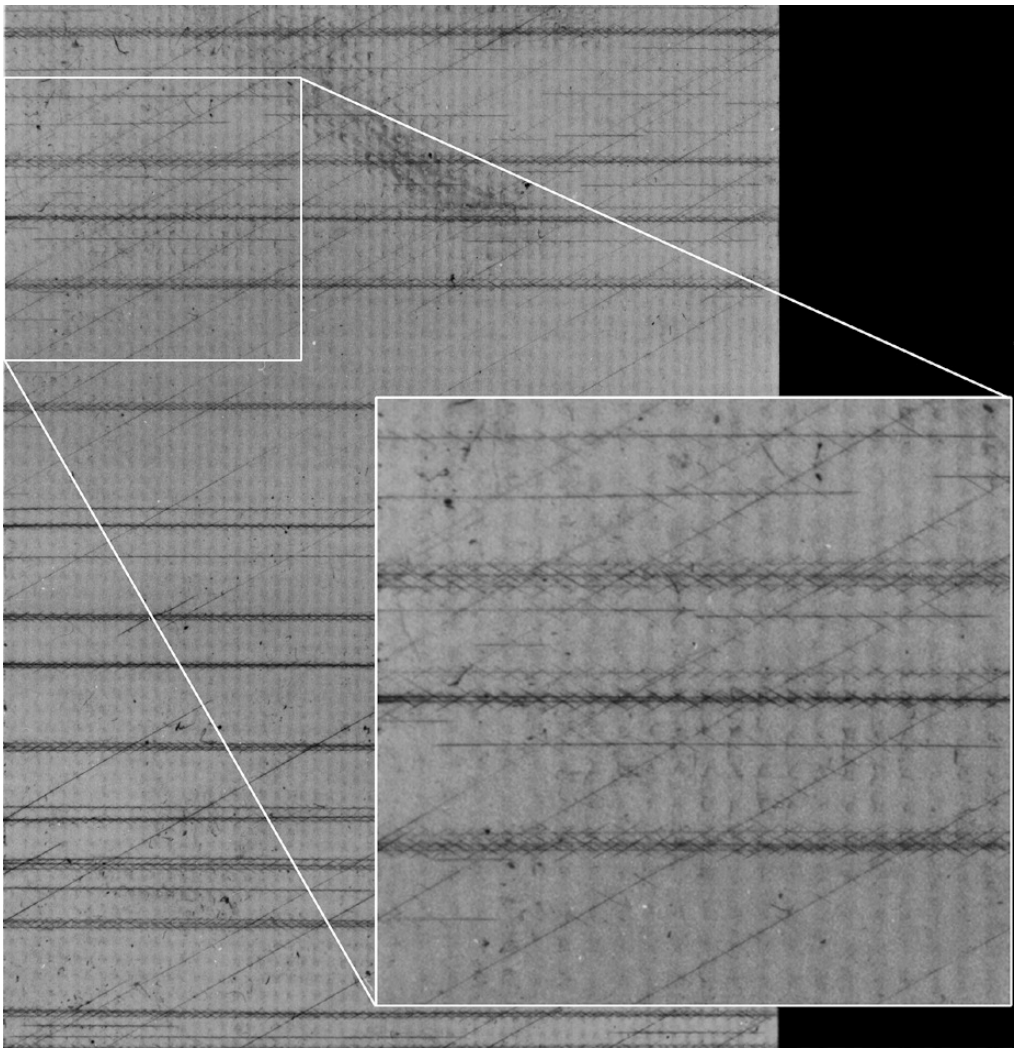

Figure 19. X-radiograph of the sublaminate-level scaled $[(+60/-60/90_2)_2]_s$ layup. Applied stress was 75 MPa. Damage consists of 90° ply matrix cracks and immediate formation of short, stich-like, -60° and +60° ply matrix cracks in all remaining 60° plies. The very long cracks are at the surface in the +60° plies.

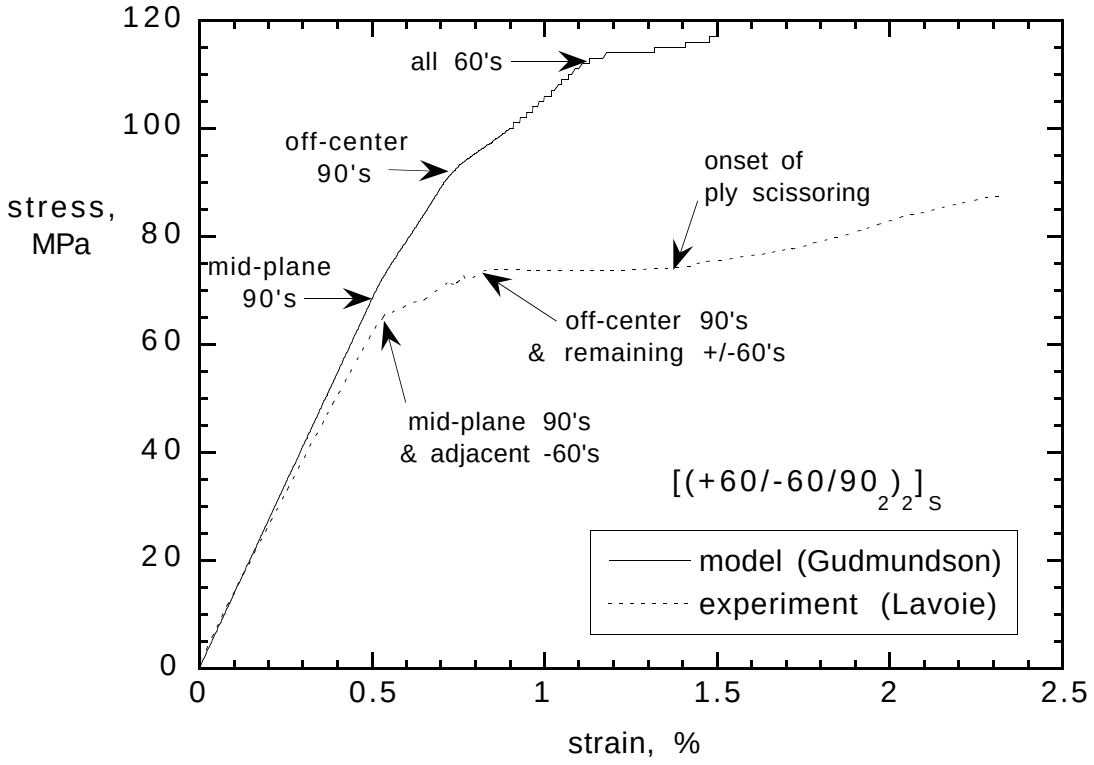

Figure 20. Modeled (solid line) and actual (dashed line) stress-strain response of the sublaminate-level scaled $[(+60/-60/90_2)_2]_s$ layup. Arrows indicate the onset of matrix microcracking in the various plies, or ply groups.

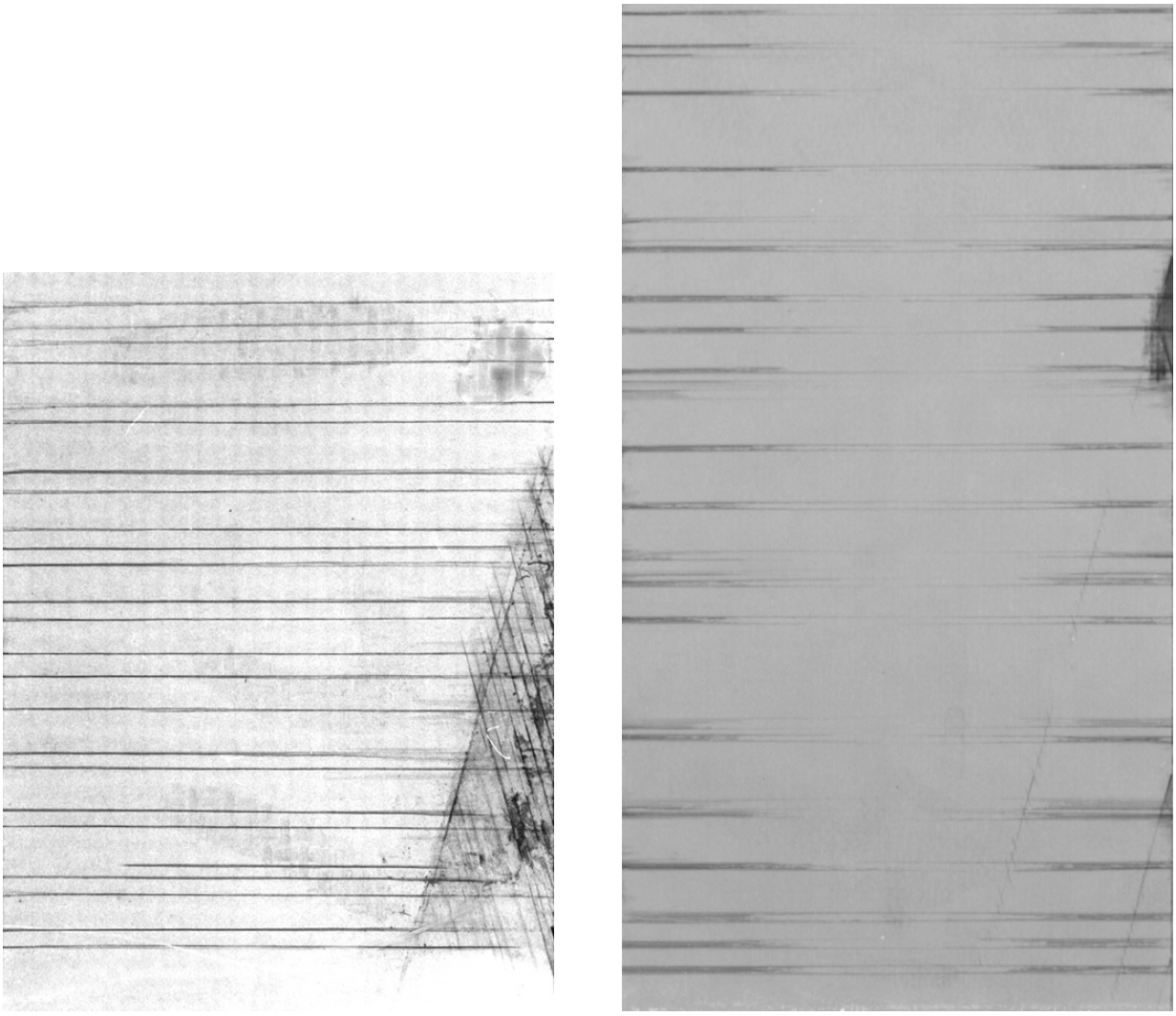

(a) (b)

Figure 21. An x-ray of a captured +15° delamination in an (a) n=1 size $[+15/-15/90_2]_s$ layup, loaded to 398 MPa. (b) n=3 size $[+15_3/-15_3/90_6]_s$ layup, loaded to 192 MPa.

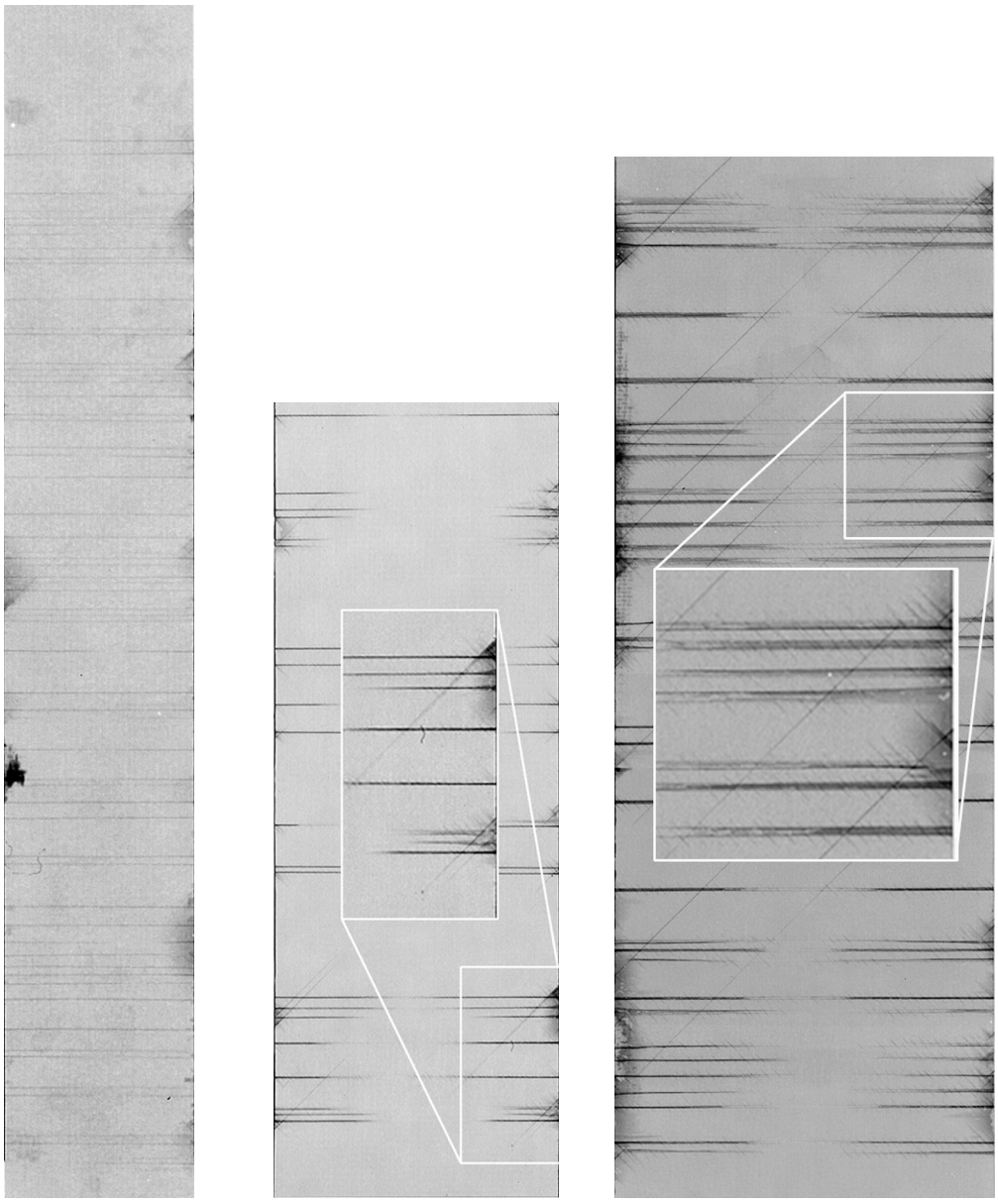

(a) (b) (c)

Figure 22. Three sizes of $[+45_n/-45_n/90_{2n}]_s$ shown at stresses very near their respective failure stress. Several +45° delaminations appear before ultimate failure in (a) n=1 size at 147 MPa, and 105% of average failure stress in (b) n=2 size at 103 MPa, or 123% of average failure stress, and in (c) n=3 size at 69 MPa, or 87% of average failure stress.

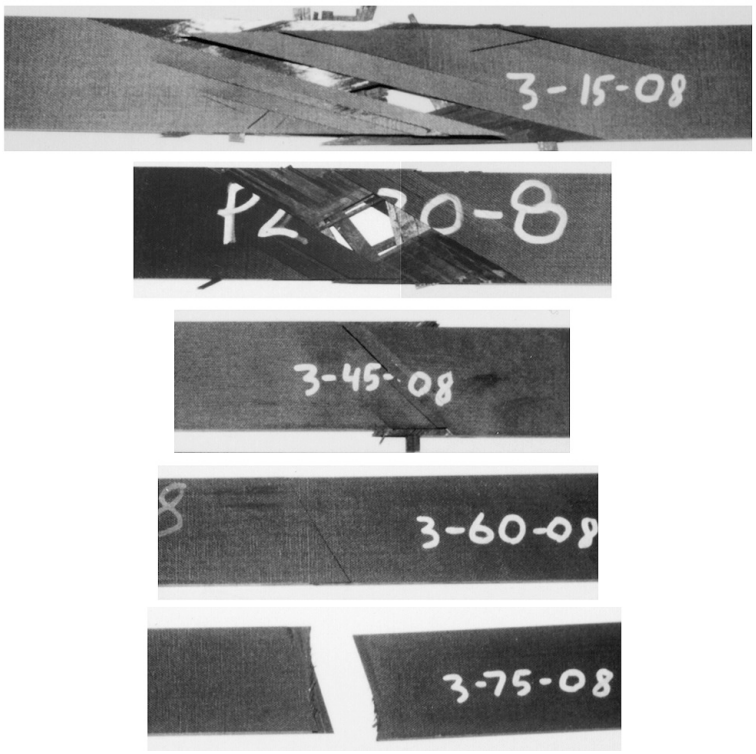

Figure 23. Photographs of failed $[+\theta_3/-\theta_3/90_6]_s$ laminates.

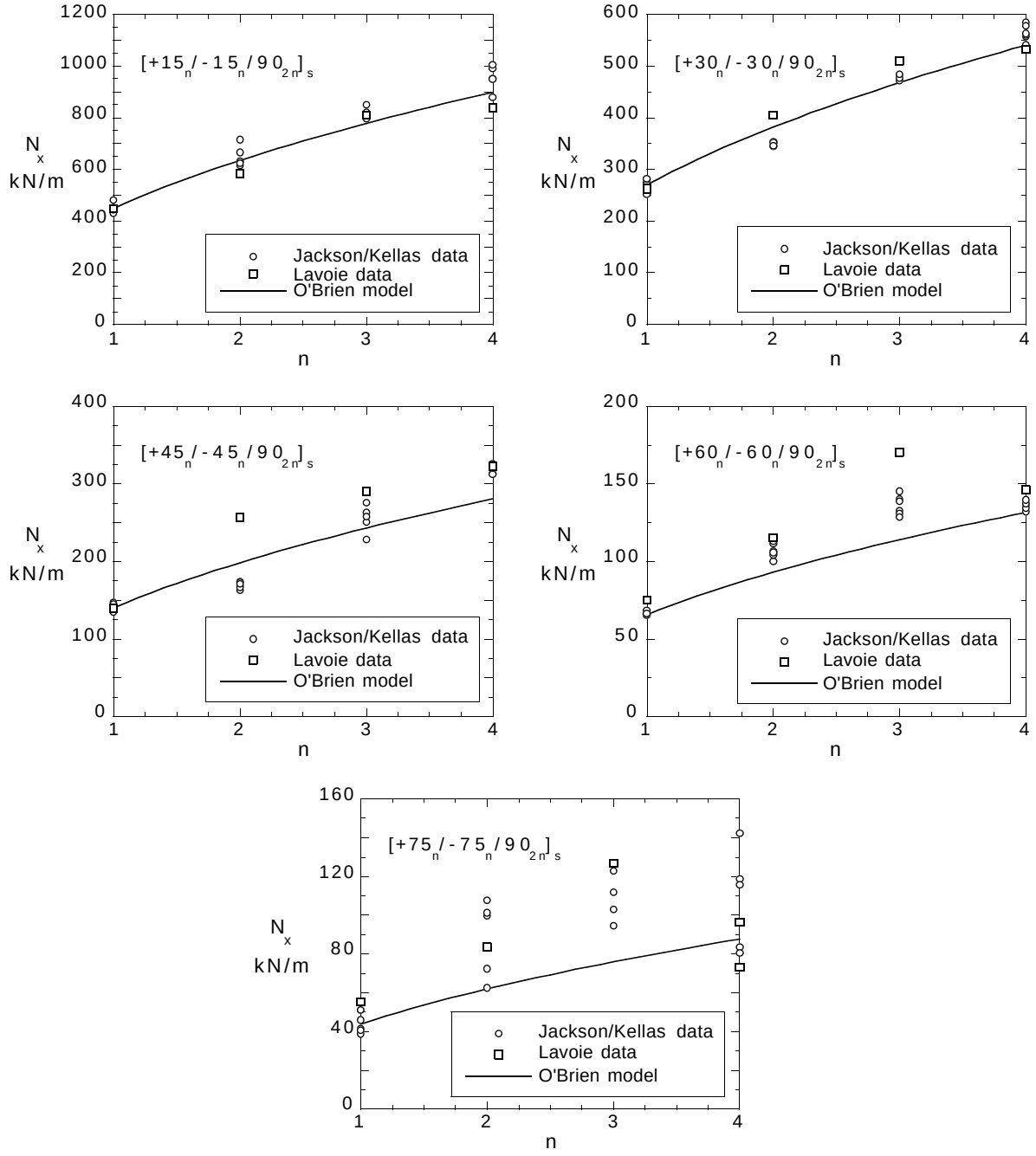

Figure 24. The strength scaling (displayed as a force-resultant) of $[+\theta_n/-\theta_n/90_{2n}]_s$ AS-4/3502 carbon/epoxy laminates is effectively predicted using a strain-energy release rate model for delamination. Experimental data from Jackson and Kellas (1993) (circles), one year later by Lavoie (diamond), and O'Briens (1993) model (line).